

SILVER DENDRITE BASED THREE-DIMENSIONAL SURFACE
ENHANCED RAMAN SCATTERING (SERS) SUBSTRATES

by

SANDESH RAJKUMAR SHELKE

Presented to the Faculty of the Graduate School of

The University of Texas at Arlington in Partial Fulfillment of

the Requirements

for the Degree of

MASTER OF SCIENCE IN MATERIALS SCIENCE AND ENGINEERING

THE UNIVERSITY OF TEXAS AT ARLINGTON

May 2016

Copyright © by SANDESH RAJKUMAR SHELKE 2016

All Rights Reserved



ACKNOWLEDGEMENTS

It is my pleasure acknowledging my supervisor, Dr. Yaowu Hao for the opportunity he has given me to learn and develop my abilities under his supervision during my research. I always recognize his encouragement and useful advice throughout obstacles which are the nature of any research environment. I also appreciate the fact that despite difficulties he was willing to provide financial support that helped me to focus on my research.

I am very lucky to have so many excellent members like Sina, Akshay, Chris and Aaron, in our group, they provided their kind help without any reservation when I needed it most. This thesis work would be difficult to have been completed on schedule without their patient and support.

Moreover, my thanks to CCMB and Nanofab, where they provide most of advanced facilities for my project. I also appreciate Dr. Fuqiang Liu and Dr. Kyungusk Yum for serving in my thesis committee.

Last but not least, I want to show gratitude to my parents, friends and my ladylove. Sincere thanks to my parents for the financial support and friends who took care of my daily needs, supporting me during my long hours in the lab. And my parents and ladylove to continuously motivating and helping me in my studies at UTA.

May 16, 2016.

ABSTRACT

SILVER DENDRITE BASED THREE-DIMENSIONAL SURFACE ENHANCED RAMAN SCATTERING (SERS) SUBSTRATES

Sandesh Rajkumar Shelke, M.S.

The University of Texas at Arlington, 2016

Supervising Professor: Yaowu Hao

Three-dimensional (3D) hierarchical nanostructures have been considered as one of the most promising surface-enhanced Raman spectroscopy (SERS) substrates because it provides high-density hotspots along the three-dimension directions and high surface areas.

In this thesis, we report the synthesis process to develop 3D SERS substrates in thin wall quartz capillary tube on Cu wire. These 3D SERS substrates consist of Ag dendrite, Au-Ag and Pd-Ag bimetallic nanostructures which was synthesized by employing simple galvanic replacement reactions (GRR). In this synthesis process Cu wire which is used as substrate was inserted in the thin walled quartz capillary tube and then AgNO_3 was injected into the tube to form Ag dendrite on the Cu wire substrate. This pre-prepared dendrite was used to prepare bimetallic nanostructures of Au-Ag and Pd-Ag by injecting chlorauric acid (HAuCl_4) and palladium chloride (PdCl_4) into the tube, respectively. The GRR process leads to the replacement of Ag atoms by

Au and Pd which causes corresponding morphological change of the underlying Ag dendrite. The GRR leaves pores where Ag is depleted. The morphological and compositional changes caused by GRR was analyzed by using scanning electron microscopy (SEM) and energy-dispersive X-ray spectroscopy (EDX). Two close metallic surfaces can enhance the electromagnetic (EM) field around molecules absorbed between them, which leads to extremely high SERS enhancement. These 3D SERS substrates was tested in detection of aqueous 4-Mercaptobenzoic Acid (4-MBA) solution with various concentrations. The fabricated substrate was employed to detect the 4-MBA solution to the detection limit down to 10^{-13} M and exhibits high-enhanced performance. The results indicated that these 3D unique bimetallic nanostructures can amplify Raman signals for extremely low concentration molecules as compared to the Ag dendrite nanostructure substrates.

TABLE OF CONTENTS

ACKNOWLEDGEMENTS.....	iii
ABSTRACT	iv
TABLE OF CONTENTS.....	vi
LIST OF ILLUSTRATIONS	ix
CHAPTER 1	13
INTRODUCTION	13
CHAPTER 2	16
BACKGROUND INFORMATION.....	16
2.1 PLASMONIC NANOSTRUCTURES	16
2.1.1 FUNDAMENTAL PLASMON PROPERTIES.....	16
2.1.2 PRINCIPLE OF SURFACE PLASMON RESONANCE (SPR)	17
2.2 RAMAN SPECTROSCOPY AND SURFACE ENHANCED RAMAN SCATTERING	20
2.2.1 RAMAN SPECTROSCOPY	20
2.2.2 SURFACE-ENHANCED RAMAN SPECTROSCOPY	26
2.2.3 SERS SUBSTRATE.....	27
2.2.4 THREE-DIMENSIONAL (3D) SERS SUBSTRATE	28
2.3 SILVER NANOPARTICLE AND THEIR NANOSTRUCTURE	29
2.3.1. SILVER DENDRITES.....	32
2.4 VARIOUS SYNTHESIS METHODS FOR AG DENDRITES.....	32

2.4.1 GALVANIC REPLACEMENT METHOD.....	33
2.5 BIMETALLIC NANOSTRUCTURES.....	35
2.5.1. GALVANIC REPLACEMENT REACTION (GRR) METHOD FOR SYNTHESIS OF BIMETALLIC NANOSTRUCTURE.....	36
2.5.2 ALLOYING VS DEALLOYING PROCESSES IN GRR.....	38
CHAPTER 3	42
EXPERIMENTS AND RESULTS.....	42
3.1 CHEMICALS AND MATERIALS.....	42
3.2 AG DENDRITES INSIDE THE CAPILLARY TUBE.....	42
3.2.1. SYNTHESIS.....	42
3.2.1.1 MECHANISM OF FORMING SILVER DENDRITES.....	44
3.2.2 CHARACTERIZATION.....	46
3.2.2.1 SCANNING ELECTRON MICROSCOPY (SEM) AND ENERGY- DISPERSIVE X-RAYS (EDX)	46
3.2.2.2 SERS Results	49
3.3. Au-Ag DENDRITES IN THE CAPILLARY TUBE.....	51
3.3.1 SYNTHESIS.....	51
3.3.2. CHARACTERIZATION OF Au-Ag NANOSTRUCTURES	52
3.3.2.1. SCANNING ELECTRON MICROSCOPY (SEM) AND ENERGY-DISPERSIVE X-RAYS (EDX).....	52
3.3.2.2 SERS RESULTS.....	55
3.3.3 MECHANISM OF FORMING Au-Ag NANOSTRUCTURES.....	57

3.4 Pd-Ag DENDRITES IN THE CAPILLARY TUBE.....	59
3.4.1 SYNTHESIS.....	59
3.4.2 CHARACTERIZATION OF Pd-Ag NANOSTRUCTURES	59
3.4.2.1. SCANNING ELECTRON MICROSCOPY (SEM) AND ENERGY-DISPERSIVE X-RAYS (EDX).....	59
3.4.2.2 SERS RESULTS.....	62
3.4.3 MECHANISM OF FORMATION OF Pd - Ag NANOSTRUCTURE.	64
CHAPTER 4	66
CONCLUSION.....	66
REFERENCES	69
BIOGRAPHICAL INFORMATION.....	77

LIST OF ILLUSTRATIONS

Figure 1: Schematic of plasma oscillation in a metal particle induced by Electromagnetic Wave. [76].....	17
Figure 2: Model Molecule in Raman System.	21
Figure 3 : (A) Energy level diagram for ground state and the virtual energy level. Green arrows is Rayleigh scattering; red arrow is anti- stokes scattering; gray arrow is stoke scattering. (B) Scattering from Interaction of Light and Molecules.	23
Figure 4 : Schematic of Raman Spectroscope.	24
Figure 5 Illustration of Surface enhanced Raman Scattering (SERS)	27
Figure 6: 3D hierarchical ZnO/Si nanomace SERS substrates [3].....	29
Figure 7 : Schematic illustration of the morphological and structural changes at the different stages of the galvanic replacement reaction between an Ag nanoparticles and H ₂ AuCl ₄ in an aqueous solution [87].	38
Figure 8: Schematic of the morphological and structural changes involved in galvanic replacement reaction between Ag nanocube and Pd ²⁺ and Pt ²⁺ ions [87].	39
Figure 9: Schematic illustration of dealloying that involved the use of H ₂ AuCl ₄ . [87]	41
Figure 10: Schematic illustration of galvanic replacement reaction between an Ag cuboctahedron and H ₂ AuCl ₄ [87].	41
Figure 11 : Thin walled quartz capillary tube	43
Figure 12 : Syringe with quartz capillary tube	43
Figure 13 : Schematic of the galvanic replacement reaction in the capillary tube for Ag dendrite formation. (A) Capillary tube with Cu wire immediately	

after the injection of the AgNO₃ solution. (B) After the galvanic replacement reaction which had proceeded for 5 min.....45

Figure 14: The mechanism for forming Ag Dendrites on the Top of Cu wire substrate.....46

Figure 15 : Thin wall Quartz capillary tube with Ag dendrite formed on the Cu wire48

Figure 16: SEM and EDX images of the Ag dendrite formed on the Cu wire surface in the Capillary tube. (A) Top part, (B) Middle part and (C) Bottom part.49

Figure 17: Raman Spectrum of the 4 MBA (1.0×10^{-5} M) aqueous solution on the as prepared Ag dendrite on the Cu wire in the capillary tube.50

Figure 18: SERS spectra of 4- MBA from concentration from 10^{-2} M till 10^{-8} M in acquired from Ag dendrite in the capillary tube.....51

Figure 19: SEM and EDX images of Au-Ag dendrite formed on the Cu wire at the top part of the capillary tube52

Figure 20: SEM and EDX images of Au-Ag dendrite formed on the Cu wire at the middle part of the capillary tube.....54

Figure 21: SEM and EDX images of Au-Ag dendrite formed on the Cu wire at the bottom part of the capillary tube55

Figure 22: Raman Spectrum of the 4 MBA (1.0×10^{-5} M) aqueous solution on the as prepared Au-Ag nanostructure on the Cu wire in the capillary tube...56

Figure 23: SERS spectra of 4- MBA from concentration from 10^{-2} M till 10^{-12} M is acquired from Au-Ag dendrite in the capillary tube.57

Figure 24 Schematic diagram of Au- Ag nanostructure synthesis by GRR...58

Figure 25: SEM and EDX images of Pd-Ag dendrite formed on the Cu wire at the top part of the capillary tube.60

Figure 26: SEM and EDX images of Pd-Ag dendrite formed on the Cu wire at the middle part of the capillary tube.....61

Figure 27: SEM and EDX images of Pd-Ag nanostructure formed on the Cu wire at the bottom part of the capillary tube.....62

Figure 28 : Raman Spectrum of the 4 MBA (1.0×10^{-5} M) aqueous solution on the as prepared Pd-Ag dendrite on the Cu wire in the capillary tube.....63

Figure 29: SERS spectra of 4- MBA from concentration from 10^{-2} M till 10^{-13} M in acquired from Pd-Ag dendrite in the capillary tube.64

Figure 30: Schematic diagram of Pd- Ag nanostructure synthesis by GRR .65

LIST OF TABLES

Table 1: Comparison of the Suitability of Different Metals for Plasmonic Applications [30].	30
Table 2: Summary of the Shapes, LSPR Absorption Peaks, Demonstrated Applications, and Methods for Synthesis of Ag Nanostructures [30].	31
Table 3 : Reduction potentials of metals relative to the standard hydrogen electrode (SHE) [87].	34

CHAPTER 1

INTRODUCTION

Surface enhanced Raman Scattering (SERS) is a technique which determines enhanced Raman signal from Raman active-molecule that is adsorbed to an appropriate metal nanostructure surface. This technique has high level of sensitivity and high spectroscopic precision. Thus it has become very important tool for chemical and biological sensing [1].

SERS effect arises from both electromagnetic and electronic field mechanism. The SERS effect can be explained by the surface plasmon resonance (SPR) phenomenon. In general SPR, refers to the electrons that will stimulate oscillation in a metal when irradiated by electromagnetic waves. An applied external electric field by the light source causes the free electrons on the surface of the metal to oscillate collectively which give rise to the surface plasmon. As free electrons can be considered as particles with electric charge, on vibration they produce electric field. When the electric field from the vibration of free electrons and the applied external electric field (e.g., electromagnetic waves) resonate the resulting phenomenon is referred to as SPR that takes place at the surface of the metal. Hence, when the SPR frequency of particles match the illuminating light frequency the Raman signal hugely enhanced. The Raman signal enhancement highly depends on the arrangement and morphology of the particles and the frequency of the incident light.

For practical applications, it is desired for a robust SERS substrate to possess not only high density hotspots to ensure high sensitivity but also the uniform distribution of

hotspots to achieve good signal reproducibility. Recently, extensive research is being carried out to fabricate various nanostructures for SERS substrates, such as zero-dimensional (0D) clusters (Au or Ag nanospheres, nanocubes), 1D building block (nanowires, nanorods, nanotips), 2D planar substrates (nanoplates, rough metal surface), and 3D frameworks (nanoarrays, dendrites, nanoflowers, branched nanotrees, nanobutterfly wing). Among various metal nanostructures, silver nanoparticles (AgNPs) are investigated thoroughly as it has highest plasmonic ability and they are cheaper than other precious metals. The AgNPs have been synthesized in various shape such as cubes, rods, wires, disks, triangles, prisms and dendrites [2].

Most recently, 3D nanostructures with well controlled hierarchical morphologies have attracted considerable attention. Compared with other conventional SERS substrates, 3D nanostructures are far superior due to the fact that they have the potential to further expand the arrangement of hotspots along the third dimension, which could in turn increase the hotspot density and uniformity. In addition, the 3D substrates can also supply larger surface area for adsorbing more probe molecules [3].

As one well-defined 3D nanostructure, Ag dendrite consists of many multi-level branching nanostructures. It not only provides large specific surface area which is more favorable to absorption of probe molecules, but also the strong electromagnetic (EM) coupling can be formed in the space between two adjacent branches from the coupling of SPR. A large amount of 'hot spots' would exist in the spaces at the end of branches or among adjacent Ag branches. Therefore Ag dendrite shows significant potential as 3D SERS substrates [4-10], and also for other application such as catalytic [11-13], bio-sensing [14, 15], and superhydrophobic surfaces [16, 17] applications.

In addition, growing attention in recent years has been paid towards bimetallic nanostructure which comprised of noble metals such as gold (Au), silver (Ag), platinum (Pt), and palladium (Pd) due to their fascinating properties and wide range of applications. Bimetallic dendrite exhibits excellent SERS activity, combining with corresponding monometallic counterpart activity and providing intermetallic interfaces due to which pure enhancement of activity is obtained. Apart from this they allow us to change the activity by tuning the composition ratios and morphology. Also, bimetallic composition allows a more economical build-up of nanostructure. As the internal parts of this expensive metal structure are inaccessible to the analyte molecules, instead of building whole structure with expensive metals like Pd or Au, bimetallic compound can be coated specifically at the accessible top part with relatively low cost substrate. Galvanic replacement reaction (GRR) is the easiest and effective way to obtain bimetallic nanostructures [18].

In this thesis, we report the synthesis process to develop 3D SERS substrates in thin wall quartz capillary tube on Cu wire. This 3D SERS substrates consist of Ag dendrite, Au-Ag and Pd-Ag bimetallic nanostructure which was synthesized by employing GRR. These SERS substrates were tested in detection of aqueous 4-Mercaptobenzoic Acid (4-MBA) solution with various concentrations. The results indicated that these 3D unique bimetallic nanostructures can amplify Raman signals for extremely low concentration molecules as compared to the Ag dendrite nanostructure substrates.

CHAPTER 2

BACKGROUND INFORMATION

2.1 PLASMONIC NANOSTRUCTURES

In last decade, the plasmonic nanostructures has been paid great attention due to large number of potential applications in optical device, bio-sensing and surface enhanced Raman scattering (SERS). It is well known that the properties and applications of plasmonic nanostructures are heavily dependent on their size, shape, morphology, and crystallinity [19].

2.1.1 FUNDAMENTAL PLASMON PROPERTIES

Plasmon consists of a collective oscillation of conduction electrons excited by the electromagnetic field of light. The plasmon oscillation can be visualize by considering a metal particle placed in the uniform external electric field. The conduction electrons inside particle moves from one side to the other side at a specific frequency, which is called plasma frequency. The change in the external electric field and charged electrons causes “overshoot” phenomenon [20]. The quantization of this collective excitation of the conductive electron gas in a metal is also called plasmon as illustrated in Figure 1.

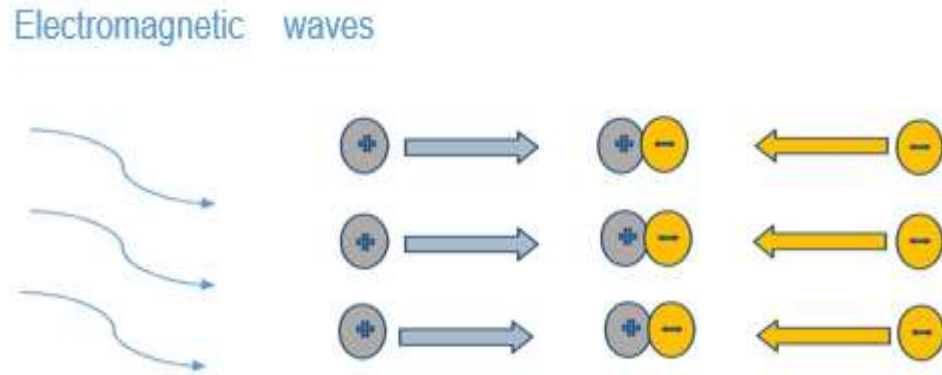


Figure 1: Schematic of plasma oscillation in a metal particle induced by Electromagnetic Wave. [76]

The plasmon plays important role in the optical properties of metal nanostructures. For bulk metals, plasma frequency lies in the ultraviolet spectrum which is higher than the frequency of visible light, so they are highly reflective, appearing white (metal) color. The fact that metals such as copper and gold have their particular colors is because their electronic inter band transitions lies in the visible range.

The surface property of the materials largely affects the position and intensity of plasmon absorption. Different plasmonic modes can be obtained by modification of plasmonic materials structure [21].

2.1.2 PRINCIPLE OF SURFACE PLASMON RESONANCE (SPR)

In general, the surface plasmon resonance (SPR) refers to the electrons that will stimulate oscillation in a metal when irradiated by electromagnetic waves [22]. An applied external electric field by the light source causes the free electrons on the surface of the metal to oscillate collectively which give rise to the surface plasmon. As free electrons can be considered as particles with electric charge, on vibration they produce electric

field. When the electric field from the vibration of free electrons and the applied external electric field (e.g., electromagnetic waves) resonate the resulting phenomenon is referred to as SPR that takes place at the surface of the metal.

For metal nanoparticles, when light irradiated on the nanoparticles and the size of nanoparticles is much smaller than the wavelength of the light, the collective oscillation of plasma would be localized near the surface. Also the resonance frequency would shift from the plasma frequency to the surface plasmon resonance frequency [23]. The plasma oscillations in the metal generally occurs in the ultraviolet (UV) region. However, in the case of Au, Ag, and Cu, the plasma shifts nearer to the visible light domain. At SPR frequency, these nanoparticles strongly enhance the scattering and absorption of the visible and near infrared (NIR) lights [24]. For example SPR peaks for gold nanoparticles with diameter about 50 to 100nm are centered at around 550nm.

SPR phenomenon can be well explained by the first Maxwell equation and Gauss's law, which can be expressed as:

$$\nabla \times D = p_f$$

Where, D is the electric displacement; p_f is the free charge density.

We can consider that the particle size is much smaller than the wavelength of light and the particles are homogeneous. Under the electric fields, the Laplace equation can be used to obtain the potentials inside and outside the particles.

$$\Phi_{in} = - \frac{3\varepsilon_m}{\varepsilon + 2\varepsilon_m} E_0 r \cos \theta \quad (2-1)$$

$$\Phi_{out} = - E_0 r \cos \theta + \frac{p}{4\pi\varepsilon_0\varepsilon_m a^2} \quad (2-2)$$

where ϵ_m is the dielectric constant of medium and ϵ is dielectric constant of the metal sphere; E_0 is external field and r is position vector at point P; a is radius of the sphere; p is the dipole moment with the form:

$$p = 4\pi\epsilon_0\epsilon_m\alpha^3 \frac{\epsilon - \epsilon_m}{\epsilon + 2\epsilon_m} E_0 \quad (2-3)$$

Also we can refer polarizability α through, $p = \alpha\epsilon_0\epsilon_mE_0$ then α can written as:

$$\alpha = 4\pi\alpha^3 \frac{\epsilon - \epsilon_m}{\epsilon + 2\epsilon_m} \quad (2-4)$$

Therefore, the equation above could be re-written as:

$$\alpha = (1 + \kappa)\epsilon\Omega \frac{\epsilon - \epsilon_m}{\epsilon + (1 + \kappa)\epsilon_m} \quad (2-5)$$

Where, Ω is referred to the volume of the particle. It is obvious that dipolar polarizability α could get the biggest value when $Re[\epsilon(w)] = -\kappa\epsilon_m$, while κ is referred to a shape factor, which represents geometrical polarizability for the surface. We can use the electron oscillations to explain it. Tiny nanostructures shape factor would have an enhancement of dipolar polarizability that explains why they could enhance LSPR intensity [25]. Thus to achieve a significant enhancement of absorption and scattering exact size of nanoparticles must be considered.

In summary, SPR in nanometer-sized structures is called Localized Surface Plasmon Resonance (LSPR). LSPR is generated when light wave trapped inside the conductive nanoparticles (NPs) with sizes smaller than wavelength of light. The phenomenon occurs as a result of interaction between the incident light and surface electrons in a conduction band. This interaction generates coherent localized plasmon oscillation with resonant frequency that varies with size, shape, composition, dielectric environment and separation distance between the NPs.

2.2 RAMAN SPECTROSCOPY AND SURFACE ENHANCED RAMAN SCATTERING

2.2.1 RAMAN SPECTROSCOPY

Raman spectroscopy is a spectroscopic technique used to examine vibrational, rotational, and other low-frequency modes in a system. In Raman spectroscopy the interaction between laser beam and molecules result in vibrational excitation or the energy of the laser photons being shifted up or down. The shift in energy gives information about the vibrational modes in the system.

When a beam of the light impinged upon the molecule, the photons of the light are absorbed by the molecules and scattered both elastically and inelastically. Elastic scattering is known as Rayleigh scattering and inelastic scattering is called Raman scattering [26].

Raman scattering is typically very weak. The light can be treated as an electromagnetic wave and molecule treated as tiny spheres connected by the spring as shown in the Figure 2.

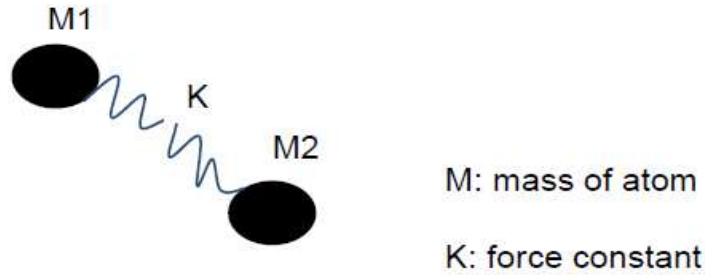


Figure 2: Model Molecule in Raman System.

The electric field of incident light can be specified as

$$E(x, t) = E_0 + \cos(\omega t - kx)$$

When a molecule is placed in the electric field, it generates an induced dipole moment because its positively charged nuclei are attracted toward the negative pole and its electrons are attracted toward the positive pole of the field.

The dipole moment P , induced in molecule by the external electric field E , is proportional to the field as shown

$$P = \alpha E$$

E at a particular location can be written as

$$E = E_0 \cos(2\pi V_0 t)$$

where V_0 is incident light frequency, Substituting these above equations to give induced dipole moment

$$P = \alpha E_0 \cos(2\pi V_0 t)$$

For most molecular bonds, the single atoms are restricted to specific vibrational modes. The vibrational energy of mode is quantized and can be expressed as

$$E_{vib} = \left(j + \frac{1}{2} \right) hV_{vib}$$

where j is vibrational quantum number, V_{vib} is the frequency of the vibrational mode, and h is Planck constant.

When the incident light illuminated the matter, the electromagnetic wave will induce an oscillation dipole moment and leads to virtual energy state. Usually, the vibrational quanta is smaller than the energy level of the virtual state. During interaction of photons and molecules, there are two possible results either the material will lose or absorbs energy and emit the photons. When the emitted photon energy is lower than absorbed photon energy, some of the energy of the incoming photon is absorbed by the molecules and longer wavelength is emitted, this is stokes scattering. When the emitted photons have higher energy than absorbed photons energy then short wavelength is emitted, this is anti-stokes scattering. The Raman scattering consist of both stokes and anti-stokes scattering. When the emitted photons energy and absorbed photon energy is same. This is Rayleigh scattering. As shown in Figure 3, the Raman scattering occurs when incident light is scattered from an individual molecule or atom and it results from electric polarizability of the atoms [26].

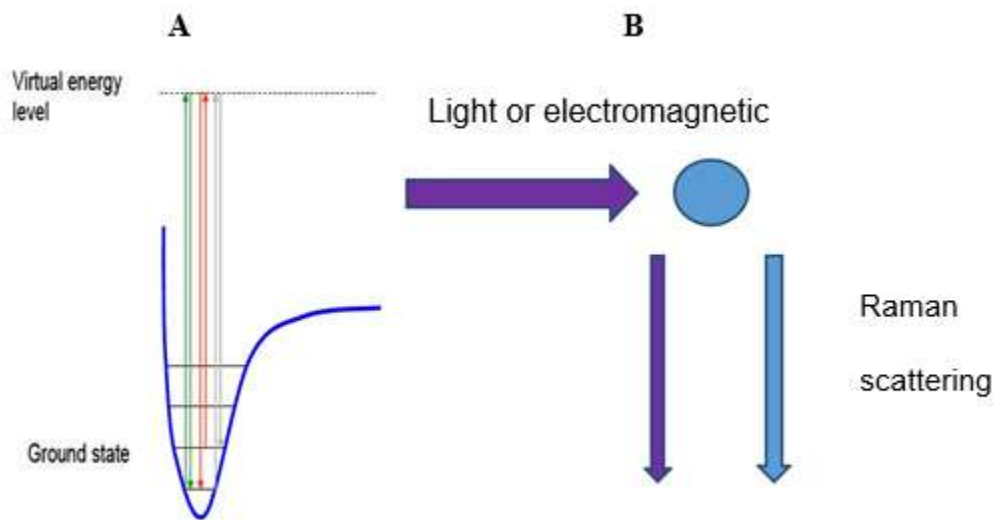


Figure 3 : (A) Energy level diagram for ground state and the virtual energy level. Green arrows is Rayleigh scattering; red arrow is anti- Stokes scattering; gray arrow is Stokes scattering. (B) Scattering from Interaction of Light and Molecules.

To be Raman active, a vibration mode needs to result in polarizability change in a molecule. The deformation of the electron clouds of a molecule in an external electric field is called as polarizability which is a critical factor for the Raman scattering.

Raman microscopes are commonly used tool that can examine microscopic area of material by illuminating laser beam down to the micrometer level. The schematic of the Raman spectroscopy is illustrated in Figure 4. Raman microscopy is the same as those of conventional dispersive Raman instruments, which include the following elements:

1. Excitation source (Laser).
2. Sample Illumination system and light collection optics.
3. Spectral Analyzer.
4. Detector and computer control system.

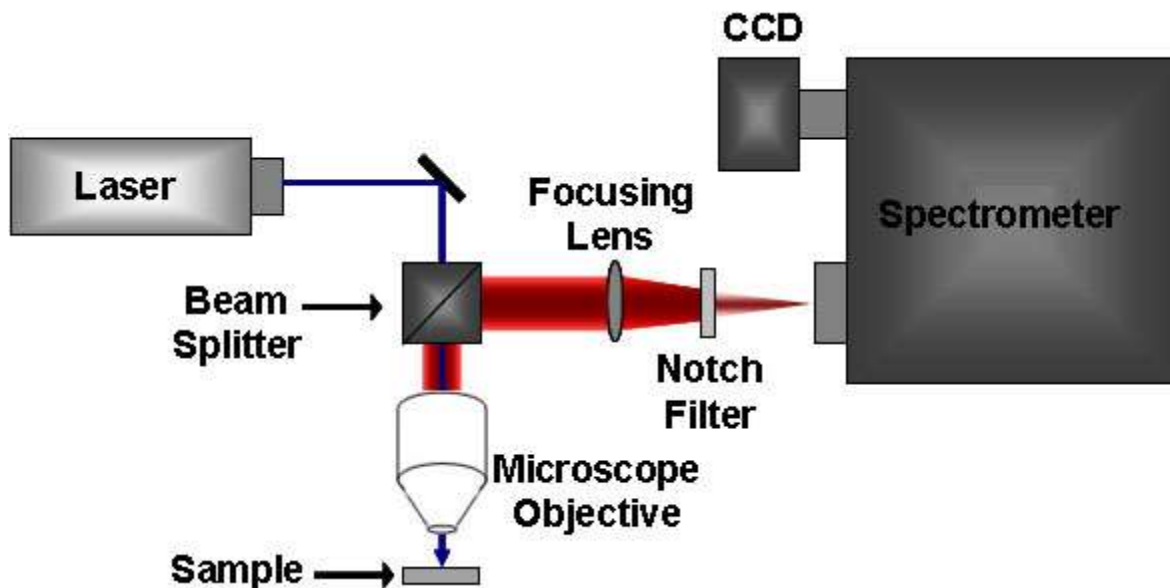


Figure 4 : Schematic of Raman Spectroscopy.

The Raman spectroscopy requires highly monochromatic light to illuminate the sample, which is easily provided by the laser source. This laser source provides stable and intense beam of radiation. Laser sources usually used are gas continuous wave lasers such as Ar, Kr and He-Ne, diode or Nd:YAG. Usually short wavelength sources such as argon ion and krypton ion lasers produce significant fluorescence and cause photodecomposition of the sample. Long wavelength sources such as diode or Nd:YAG lasers can be operated at much higher power without causing photodecomposition of sample and eliminate or reduce fluorescence in most cases.

Band pass filters are used to isolate a single laser beam. Super notch filters, rejection filters, holographic notch or edge filters and holographic filters are used to separate relatively weak Raman lines from intense Rayleigh scattered radiations before the light reaches the analyzer.

Diffraction grating is the most important component of spectral analyzer. It consist of some parallel groves on the surface that are used to disperse the Raman scattered light depending on the wavenumber of the light before this signals are recorded by the detector.

The detector is used for detecting different Raman scattered light wavelengths. It is made by photoelectric materials and converts the incoming optical signal into charge which is integrated and transferred to readout device. Charge-coupled device (CCD) is most commonly used as detector. CCD is a silicon based multichannel array detector. They are extremely sensitive to the light and thus suitable to detect weak Raman signal. They also allows multichannel operation which means that entire Raman spectrum can be detected in a single acquisition. The computer is used to calculate and plot the Raman shift with versus wavenumber for the Raman spectrum.

Fluorescence is a major problem of Raman spectroscopy. This arises because colored sample and impurities also absorbs some laser radiation and emit it as fluorescence. The fluorescence gives intensity of several thousand times higher than Raman scattered light, which might cover the Raman scattered light. To minimize the fluorescence three methods are commonly used as follows:

1. Use of high-power laser beam with prolong time to illuminate the material can help in bleaching out the impurities.
2. As Raman scattering lifetime is much shorter than fluorescence an electron gate can be used to measure the Raman signal.
3. Using a longer wavelength of laser excitation.

2.2.2 SURFACE-ENHANCED RAMAN SPECTROSCOPY

Surface Enhancement Raman Spectroscopy (SERS) was first observed in 1973 at University of Southampton, UK, by Martin Fleischman et.al.[27]. It was accidentally discovered by them when they tried to do Raman with an adsorbate of very high Raman cross section, pyridine (Py) on the roughened silver (Ag) electrode. They found that Raman signal were enhanced more than a million times. Later, it was proposed that the huge enhancement can be explained by excitation of the surface plasmon. Thus, nowadays SERS has become a technique which determines enhanced Raman signal from Raman active-molecule that is absorbed to an appropriate metal surface. This technique has high level of sensitivity and high spectroscopic precision. Thus it has become very important tool for chemical and biological sensing.

SERS effect arises from both electromagnetic and electronic field mechanism. According to electromagnetic theorem, when the wavelength of the incident light is close to the plasma wavelength of the metal, conduction electrons in the metal surface are excited into the extended surface electronic excited state called surface Plasmon resonance (SPR). Hence, when the SPR frequency of particles match the illuminating light frequency the Raman signal hugely enhanced. The Figure 5, shows the illustration of surface enhanced Raman Spectroscopy.

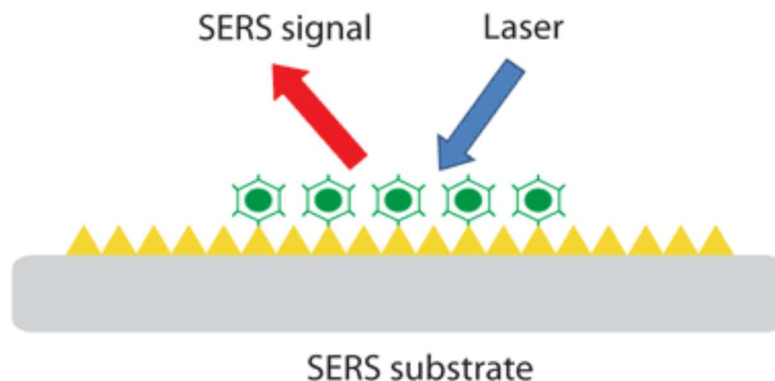


Figure 5 Illustration of Surface enhanced Raman Scattering (SERS)

2.2.3 SERS SUBSTRATE

The Raman signal enhancement highly depends on the arrangement and morphology of the particles and the frequency of the incident light. SERS active substrate fabrication is a very important field in SERS research. There are a lot of metal particles with different size and shape that can be used, especially from silver, gold and copper. However, there is a challenge for producing uniform, reproducible and highly sensitive SERS substrates.

Investigating the synthesis of metal nanoparticles with different nanostructures has been a hot topic of research due to their important applications in different areas including optics, catalysis, biomolecular imaging and SERS. Generally, there are two methods, top-down and bottom-up, were used to produce nanostructures.

As we know that when the molecules attach to the surface of metal nanoparticles the phenomenon of Raman enhancement occurs. The surface of metal nanoparticles consist of large number of 'hot spots'. Design of maximum hot spots of metal nanoparticles is an important principal for SERS design. Recently, there are a lot of

designs of 1D and 2D SERS substrates that have been reported through controlling the shape and size of metal or bimetallic nanostructures [28].

The two important factor that affects the enhancement are size and shape of metal nanoparticles (MNP). The bigger size of MNP will lead to a lower overall efficiency of the enhancement. But if the size is too small will fail to produce electrical conductivity and fail to have an enhancement for the electric field. Also, high surface area and high uniformity are important factors when preparing SERS substrates. Thus lots of research work has been carried out to prepare metal nanoparticles with ideal sizes and shapes.

2.2.4 THREE-DIMENSIONAL (3D) SERS SUBSTRATE.

For practical applications, it is desired for a robust SERS substrate to possess not only high density hotspots to ensure high sensitivity but also the uniform distribution of hotspots to achieve good signal reproducibility. The 3D nanostructures with well controlled hierarchical morphologies are good candidates as highly effective SERS substrates. Compared with other conventional SERS substrates, 3D nanostructures have the potential to further expand the arrangement of hotspots along the third dimension, which could in turn increase the hotspot density and uniformity. In addition, the 3D substrates can also supply larger surface area for adsorbing more probe molecules.

Generally, there are two principal strategies for fabricating 3D SERS substrates. The first one is the 3D self-assembly method, it is strategy which bridge the top-down and bottom-up conventional methods for fabrication of nanostructure. It provides a strategy that makes possible the patterning (in a broad sense) of nanostructures made by bottom-up synthesis; it can also use patterns generated by top-down fabrication to guide the ordering of nanostructures made by bottom-up methods. But this method suffers from

poor control and reproducibility. Another one is the template method, which consists of noble-metal nanoparticles (NPs) and their 3D nanoscaffolds. Currently, many emerging 3D SERS substrates have been widely reported by the template method. For example, the Au or Ag nanoparticles decorated anodic aluminum oxide (AAO) channels, carbon nanotubes (CNTs), titanium dioxide (TiO₂) nanoarrays, zinc oxide (ZnO) nanorod arrays. The Figure 6 shows an illustration of a 3D SERS substrate [3].

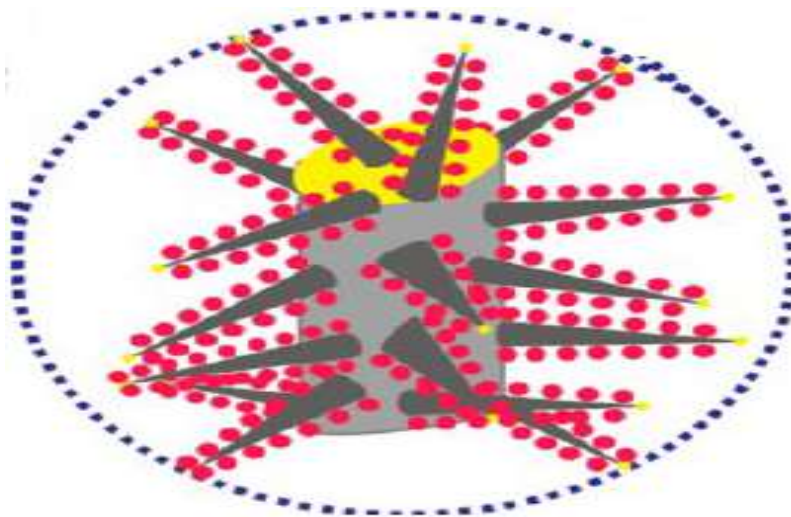


Figure 6: 3D hierarchical ZnO/Si nanomace SERS substrates [3].

2.3 SILVER NANOPARTICLE AND THEIR NANOSTRUCTURE











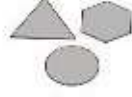


There are a lot of MNPs, especially from the silver (Ag), gold (Au) and copper (Cu), with different size and shape that can be used for SERS metal particles. Among various MNP, silver nanoparticles (NPs) are investigated thoroughly as it offers many advantages over other metals. From ancient time Ag has been used in photography and staining of biological tissues due to the black color associated with the large aggregation of the Ag - NP's. It has highest thermal and electric conductivity thus making it the best component for electrical interconnection. The most important factor of Ag in terms of plasmonic is

that it has strong surface plasmonic effect. Also, Ag is the cheapest of all other precious metals. Hence for SERS applications silver is unique, for its excellent qualities in terms of plasmonic ability, available nanostructures, and material cost.[29]

Table 1: Comparison of the Suitability of Different Metals for Plasmonic Applications [30].

Metal	Plasmonic ability	Chemical	Nanostructure formation	Cost (per ounce)
Aluminum (Al)	Good in UV region	Stable after surface passivation	Very few nanostructures; Used in lithographic patterning	\$0.049
Copper (Cu)	Interband transitions below 600nm	Easy oxidation	Very few nanostructures	\$14.8
Gold (Au)	Interband transitions below 500nm; High quality factor	Very stable, biocompatible	Many nanostructures	\$950
Palladium (Pd)	Low quality factor; Not suitable for plasmonics	Stable	Many nanostructures	\$265
Platinum (Pt)	Low quality factor; Not suitable for plasmonics	Stable	Many nanostructures	\$1,207
Silver (Ag)	Highest in quality factor;	Oxidation, biocompatibility issue	Many nanostructures	\$13.4

Table 2: Summary of the Shapes, LSPR Absorption Peaks, Demonstrated Applications, and Methods for Synthesis of Ag Nanostructures [30].

Shape	Illustration	LSPR ^a	Applications ^b	Method of Synthesis
Sphere and quasi-sphere		320 - 450	SERS; LSPR sensing; assembly	Polyol process (single-crystal); Citrate reduction (quasi-sphere)
Cube and truncated cube		400 - 480	SERS; LSPR sensing; assembly	Polyol process; Seed-mediated growth
Tetrahedron and truncated tetrahedron		350 - 450	SERS	Polyol process; Light-mediated Growth
Octahedron and truncated octahedron		400 - 500	Assembly	Polyol process; seed-mediated growth; light-mediated growth
Bar		350 - 900	SERS	Polyol process
Spheroid		350 - 900	SERS	Polyol process
Right bipyramid		500 - 700	-	Polyol process
Beam		-	Electron transport	Polyol process
Decahedron		350 - 450	-	Seed-mediated growth; light-mediated growth; citrate reduction
Wire and rod		380 - 460	Wave guiding; electronics; SERS; assembly	Seed-mediated growth
Polygonal plates and disc		350 - 1000	SERS; LSPR sensing	Light-mediated growth; polyol process
Branched structures		400 - 1100	SERS	Seed-mediated growth
Hollow structures		380 - 800	SERS; LSPR sensing	Template-directed growth

a-The main absorption peak (nm), b- Assembly means the nanostructure has been assembled into larger structures for Plasmonic applications or studies. The red lines in the illustration refer to a crystalline plane; the dark face and the light faces are {111}.

2.3.1. SILVER DENDRITES

Ag NPs are synthesized in various shape such as cubes, rods, wires, disks, triangles, prisms and dendrites [31]. Among all the structure, Ag dendrites possess many multi-level branching nanostructures, thus it provides large specific surface area and the corresponding complex nanostructure which may be more favorable to the absorption of probe molecules. Most importantly, the strong electromagnetic (EM) coupling can be formed in the space between two adjacent branches from the coupling of SPR. Thus a large amount of 'hot spots' would exist in the spaces at the end of branches or among adjacent Ag branches. Therefore Ag dendrite shows significant potential as SERS substrates [4-10].

2.4 VARIOUS SYNTHESIS METHODS FOR AG DENDRITES

A variety of methods to fabricate silver hierarchical nanostructures with diverse structural features has been employed which includes electrochemical deposition [17, 30, 32-46], electroless redox reaction [15, 47-63], wet chemical route using reducing agents in aqueous solution [51, 64-77], photocatalytic reduction [28, 78], decomposition by visible light irradiation [79], ultraviolet irradiation of surfactant micelles [80], ultrasonically assisted templated synthesis, iodination treatment to the evaporated silver foil surface [81], sonoelectrochemical deposition [12, 82-85], and photoreduction by ultraviolet irradiation [86]. However, each of this methods have some deficiencies, such as requiring special. equipment, time consuming (up to 30 days), impurity, using highly hazardous materials (e.g. HF), introduction of seed particles and templates, multiple capping agents, multiple synthetic steps, difficulties to remove the templates or surfactants from the surface of the products, high-cost or low-yield restrictions, and poor reproducibility.

By a considerable extent, wet chemical reaction, electrochemical deposition, and galvanic replacement have been the most commonly used methods for production of silver fractal nanostructures. Wet chemical technique, as one of the first choices not only for making silver dendrites but also numerous other metallic nanostructures, is based on the reduction of Ag ions in an aqueous solution using a soluble reducing agent (p-hydroquinone (HQ) [66], hydroxylamine [64], NH_2OH [65], L-ascorbic acid [67, 71, 73], p-phenylenediamine (PPD) [68], sodium tetra hydroborate (NaBH_4) [70, 74], polyaniline [8], HF [72], ethylene glycol [75], formamide [77], and so forth). Nevertheless, in most cases, surfactants and organic/inorganic moieties are inevitable to control aggregation and growth direction. Moreover, the reaction is usually conducted under special condition, requiring vigorous stirring, heating or cooling, and precise adjustment of pH. In contrast, electrochemical deposition method benefits from relatively good control over reduction and growth kinetics by adjusting applied potential, while it lacks the versatility of wet chemical and galvanic replacement techniques to produce diverse more sophisticated nanostructures without introducing more complicated templates and reagents into the reaction process.

2.4.1 GALVANIC REPLACEMENT METHOD

Among all the above synthesis methods galvanic replacement is the simple and attractive method to fabricate varied nanostructures of noble metals (such as Au, Ag, Pd, and Pt) and their alloys. Galvanic replacement is an electrochemical process that involves the oxidation of a metal (which is referred as sacrificial templates) by the ions of another metal having higher reduction potential. The Galvanic replacement method is very effective way to make MNPs due to its ability to tune the size and shape, and to change

the composition, morphology of the resultant nanostructures. Table 3, summarize the standard reduction potentials of the metals commonly used in galvanic replacement studies.

Table 3 : Reduction potentials of metals relative to the standard hydrogen electrode (SHE) [87].

Reduction reaction	E^0 (V vs. SHE) ^{a)}
$\text{Co}^{2+} + 2\text{e}^- \rightarrow \text{Co}$	-0.28
$\text{Cu}^{2+} + 2\text{e}^- \rightarrow \text{Cu}$	0.34
$\text{Rh}^{3+} + 3\text{e}^- \rightarrow \text{Rh}$	0.76
$\text{Ag}^+ + \text{e}^- \rightarrow \text{Ag}$	0.80
$\text{Pd}^{2+} + 2\text{e}^- \rightarrow \text{Pd}$	0.95
$\text{Ir}^{3+} + 3\text{e}^- \rightarrow \text{Ir}$	1.16
$\text{Pt}^{2+} + 2\text{e}^- \rightarrow \text{Pt}$	1.18
$\text{Au}^{3+} + 3\text{e}^- \rightarrow \text{Au}$	1.50

^{a)}For ideal conditions at 25 °C and 1 atm.

Accordingly, even silver nanoparticles (Ag^+/Ag $E = 0.8$ V vs. SHE) could serve as seeds and reducing agents for synthesis of more noble metal nanostructures such as gold nanostructure (Au^{3+}/Au $E = 1.5$ V vs. SHE) [87]. Although the main governing principle of galvanic replacement is very straightforward, controlling the morphology and structure of produced nanostructures have not been that easy in all cases, as they are very sensitive to the synthesis condition, comprising ion concentrations, temperature, and the initial state of the sacrificial material. Recently, the formation of silver dendrites via galvanic replacement have been reported by several studies using bulk other metals more reactive than silver (e.g. Cu [11, 47, 57, 60, 88], Mg [89], Al [15, 50, 59, 90], Zn [49, 52,

53, 56, 91], Ni [58, 62], Sn [92]) as substrates. In most of these studies, galvanic replacement (redox reaction) and silver dendrite growth generally occurred through the direct electron transfer between Ag^+ ions and the sacrificial substrate, leading to the formation of silver hierarchical structures onto the surface of the substrate or into the template containing the sacrificial material.

The diffusion-limited aggregation (DLA) model and the anisotropic crystal growth were used to explain the growth of silver nano-dendrites. The dendrite nanostructure growth by the galvanic replacement reaction (GRR) process is dependent on the thermodynamic factors and the inherent crystal structure of the material. At the beginning of this reaction, GRR will instantly initiated at the highest surface energy spots where the surface is rough (defects, stacking fault or steps) and the bulk energy of the total system tends to decline. Thus, silver particles aggregate dendritic rather than a thermodynamically stable hexagonal structure. Consequently, some byproducts (like smaller silver nanoparticles) could form and mix with the silver dendrites or special care must be taken to detach the dendrites from the substrates/templates. It can be seen that GRR is a facile, low-cost and simple synthesis process for large-scale production of clean and highly-pure silver dendrites with well-defined structures.

2.5 BIMETALLIC NANOSTRUCTURES

In recent years, growing attention has been paid towards bimetallic nanostructure which comprised of noble metals such as gold (Au), silver (Ag), platinum (Pt), and palladium (Pd) due to their fascinating properties and wide range of applications [93]. Recently several types of Ag based alloyed dendrites Ag-Au [93-95], Ag-Pd [18, 96] have

been synthesized and tested. Bimetallic dendrite exhibits excellent activity as it provides large surface area for surface reaction activity. The bimetallics also combine with corresponding monometallic counterpart activity and provide intermetallic interfaces due to which pure enhancement of activity is obtained. Apart from this they allow us to change the activity reaction by tuning the composition ratios and morphology. Bimetallic composition allows a more economical build-up of nanostructure. As the internal parts of this expensive metal structure are inaccessible to the reaction molecule. Instead of building whole structure with expensive metals like Pd or Au, bimetallic compound can be coated specifically at the accessible top part of relatively low cost substrate. Galvanic replacement reaction (GRR) is the most easy and effective tool to obtain bimetallic nanostructures [18].

2.5.1. GALVANIC REPLACEMENT REACTION (GRR) METHOD FOR SYNTHESIS OF BIMETALLIC NANOSTRUCTURE.

Galvanic replacement reaction (GRR) of Ag nanoparticles with Au has been recently studied and the reaction mechanism in this GRR to produce bimetal nanostructures has been examined. The Figure 6, shows the major steps involved in a galvanic replacement reaction of Ag with HAuCl_4 . When Ag nanoparticles are immersed in aqueous HAuCl_4 solution GRR will instantly initiated at the highest surface energy spots where the surface is rough (defects, stacking fault or steps). The Ag atoms will undergo oxidation and get dissolved in the solution as a result small holes form on the nanoparticle surface. At the same time AuCl_4^- ions in the solution capture by the electrons that are on the surface of the nanoparticles and undergoes reduction to form Au atoms on nanoparticle surface. The newly formed Au atoms tends to be deposited epitaxially on the

surface of the Ag nanoparticles (step 1 in Figure 7). This thin deposit of the Au atom on the surface of the nanoparticles prevents the underneath Ag atom from reacting with AuCl_4^- ions. But as a result of these small opening, all the species in the reaction will easily diffuse in and out of the cavity. Further accompanying Au deposition, homogeneous alloying occurs on the underneath Ag atoms (step 2 in Figure 7). This is due to the fact that homogeneous alloying is thermodynamically more stable than the mixture of segregated Au and Ag. At last complete dissolution of pure Ag takes place from the templates thus converting the nanostructure into hollow interior and the alloyed shell (step 3 in Figure 7). If further more HAuCl_4 solution is added, the AuCl_4^- ions will cause the dealloying of the Au-Ag shell. During the dealloying process large number of Ag atoms are extracted by AuCl_4^- ions that creates many lattice vacancies leading to increase in the surface free energy. To compensate this energy, the vacancies combine to form small holes in the shell. Further dealloying causes the holes size to grow bigger and thus generates hollow nanostructure with porous walls (step 4 in Figure 7), which is generally referred as nanocages. Complete dealloying leads the nanocages to fall into small fragments of pure Au (step 5 in Figure 7). This should be noted that the mechanism of GRR are not specified to either particle shape or the material. It should take place as long as there is an appropriate difference in the reduction potential between the two metals involved [97].

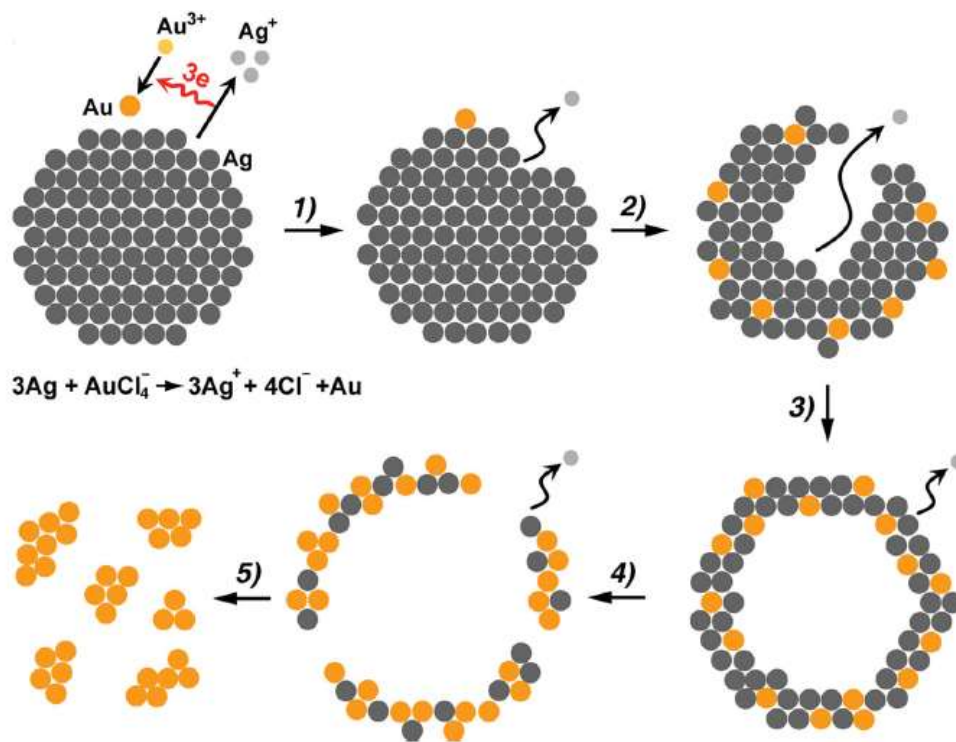


Figure 7 : Schematic illustration of the morphological and structural changes at the different stages of the galvanic replacement reaction between an Ag nanoparticles and HAuCl₄ in an aqueous solution [87].

2.5.2 ALLOYING VS DEALLOYING PROCESSES IN GRR

Alloying and dealloying are two significant processes involved in the galvanic replacement. Both the processes have high impact on the structure and morphology of the final product [97].

1. Alloying:

Alloying takes place in the initial stage of galvanic replacement reaction when thin layer of metal A is deposited on the template composed of the metal B. In general it is the basis of retaining the morphology of the original nanostructure during a galvanic replacement reaction. This could be determined by the galvanic replacement reaction between Ag nanocubes and Pd²⁺ and Pt²⁺ ions. As shown in Figure 8, reaction of Ag

nanocubes with Na_2PdCl_4 resulted in the formation of smooth, single-crystal nanoboxes composed of a Pd-Ag alloy. However, when Na_2PtCl_4 was used poly-crystalline nanoboxes with bumpy surfaces composed of Pt nanoparticles were formed. This difference in the morphology in both the cases is because Pt not easily undergoes interdiffusion over the entire surface of Ag template to form Pt-Ag alloy unlike the Au and Pd. This is attributed to the metal –metal bonding energy. As bonding energy of Pt-Pt (307 kJ mol^{-1}) is higher than the Pt- Ag (218 kJ mol^{-1}) this leads to form an island growth pattern of the Pt on the initial deposited Pt atoms on the Ag template. A relative large energy barrier for interdiffusion is also another reason. In contrast the Pd-Ag and Au- Ag alloys are favorable to form as the bonding energies of Pd-Pd (100 kJ mole^{-1}) and Au-Au (226 kJ mol^{-1}) are lower than those of Pd-Ag (137 kJ mol^{-1}) and Au-Ag (229 kJ mol^{-1}), respectively [97].

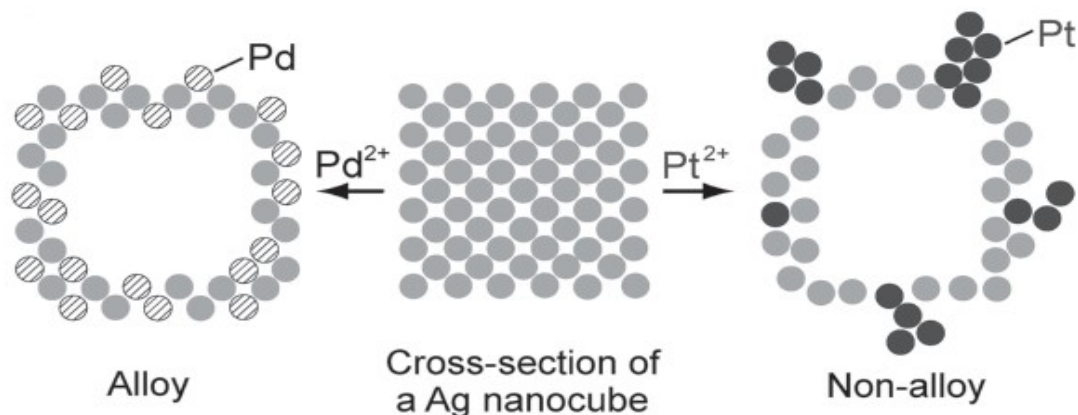


Figure 8: Schematic of the morphological and structural changes involved in galvanic replacement reaction between Ag nanocube and Pd^{2+} and Pt^{2+} ions [87].

2. Dealloying:

Dealloying takes place in the later stages of a GRR to control the porosity of the wall, when the metal with a lower reduction potential is removed from the alloyed wall. In

general the dealloying takes place by addition of more metal ions used in the galvanic replacement.

The dealloying process is explained in the Figure 9, the starting sample was prepared by the stopping the galvanic reaction between Ag nanocubes and HAuCl_4 at early stage. When more HAuCl_4 solution was added in the Au-Ag nanoboxes sample, this causes structural and morphological changes that includes

- I. Removal of the remaining Ag in the interior and closing the pores on the surface, along with the corner truncation to generate hole-free nanoboxes shown in figure 9a.
- II. By removing the Ag atoms from the Au-Ag alloyed wall nanocages with pores on the surface is generated as shown in Figure 9b.
- III. With further addition of the HAuCl_4 solution the size of the pores surface increases and then ultimately the Au structure collapses into small particles with irregular shape as shown in Figure 9c.

In contrast to the use of Ag cuboctahedron as a template, when the galvanic replacement reaction between an Ag cuboctahedron and HAuCl_4 solution occurs there are major morphological and structural changes at different stages of the galvanic replacement reaction as shown in Figure 10. The dissolution of Ag atoms takes place on the eight $\{111\}$ facets, while the deposition of Au occurs on the $\{110\}$ facets. The shape reconstruction from cubes to truncated cubes is observed in the early stage of the dealloying process for Ag nanocubes templates. This appearance of the truncation at the corner is due to a combination of both the selective deposited Au on a $\{100\}$ facets and the inherent driving force to lower the total surface free energy.

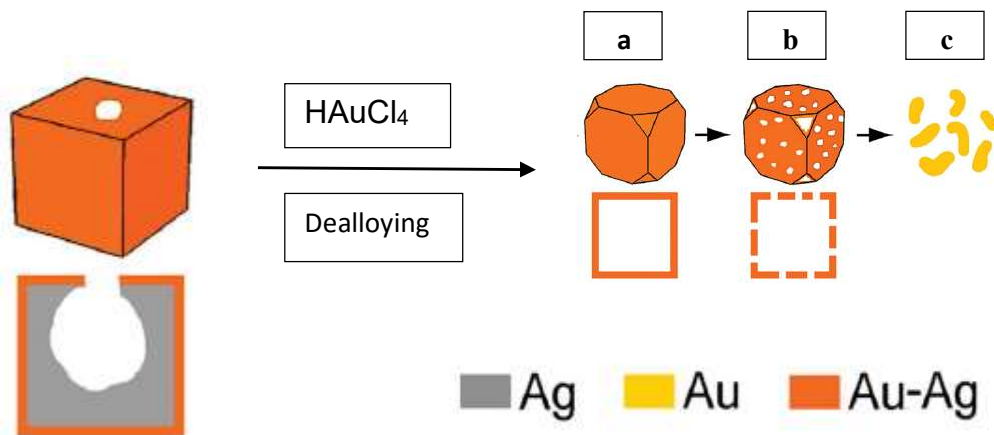


Figure 9: Schematic illustration of dealloying that involved the use of HAuCl₄. [87]

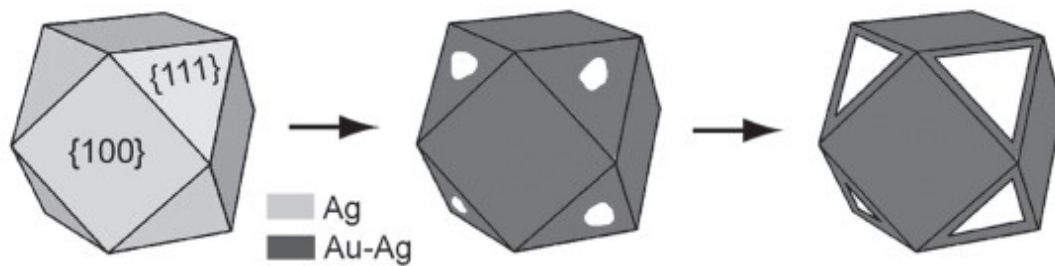


Figure 10: Schematic illustration of galvanic replacement reaction between an Ag cubooctahedron and HAuCl₄ [87].

CHAPTER 3

EXPERIMENTS AND RESULTS

3.1 CHEMICALS AND MATERIALS

Silver nitrate (AgNO_3 , 99.9%) was purchased from Alfa Aesar, Copper Bus bar wire of diameter 0.0799 mm was obtained from MSC industrial supply Co., Latex free syringe of 3 ml with BD Leur- Lok tip was purchased from BD medical, Natural Amber Latex tubing of 3.175 mm internal diameter was purchased from Amazon, Capillary Tube of Quartz with 0.2 mm internal diameter and wall thickness of 0.01m was obtained from Charles supper company, Male Leur connector of 3.175 mm was obtained from Cole-Parmer, 4-Mercaptobenzoic Acid (4-MBA), chlorauric acid (HAuCl_4) and palladium chloride (PdCl_4) from the Sigma Aldrich.

3.2 AG DENDRITES INSIDE THE CAPILLARY TUBE.

3.2.1. SYNTHESIS.

In a typical synthesis of the Ag dendrite, copper (Cu) wire 50 mm in length was cut and initially cleaned off with the ethanol solution to remove contamination and then rinsed with distilled ionized (DI) water. The Cu wire was inserted in the capillary tube through the large opening at the top of the tube.

Aqueous AgNO_3 (0.1 M) solution was taken in the syringe of volume 3 ml. The capillary tube with Cu wire inside was then attached to the syringe through leur connector and latex tubing. Figure 11 and Figure 12, show the thin walled quartz capillary tube and whole equipment for the synthesis process.



Figure 11 : Thin walled quartz capillary tube



Figure 12 : Syringe with quartz capillary tube

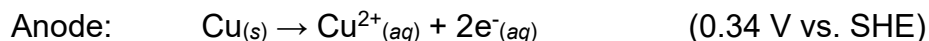
The Aqueous AgNO_3 (0.1M) solution was then slowly injected through the capillary tube for 5 minutes. To our surprise, we could obtain very pure and highly ordered Ag dendrite on the top part of the capillary tube. After formation of Ag dendrite, DI water was injected again slowly for 30 minutes through capillary tube to wash the tube thoroughly and then dried in the air.

3.2.1.1 MECHANISM OF FORMING SILVER DENDRITES.

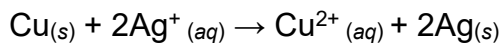
The Ag dendrites are formed galvanic replacement process of Cu replaced by Ag. When aqueous AgNO₃ solution is injected in the capillary tube with Cu wire, the Cu atoms from the surface of the wire quickly react with the Ag⁺ ions to release Cu²⁺ ions into the solution. Simultaneously Ag⁺ ions are reduced into Ag atoms and deposited on the surface of the Cu wire. As a result the original Cu wire increasingly covered by a grey precipitate of Ag. The Figure 13, shows the schematic of galvanic replacement reaction in capillary tube for Ag dendrite formation process.

The equation involved in this galvanic replacement reaction can be summarized as follows

Half reaction:



The overall reaction is:



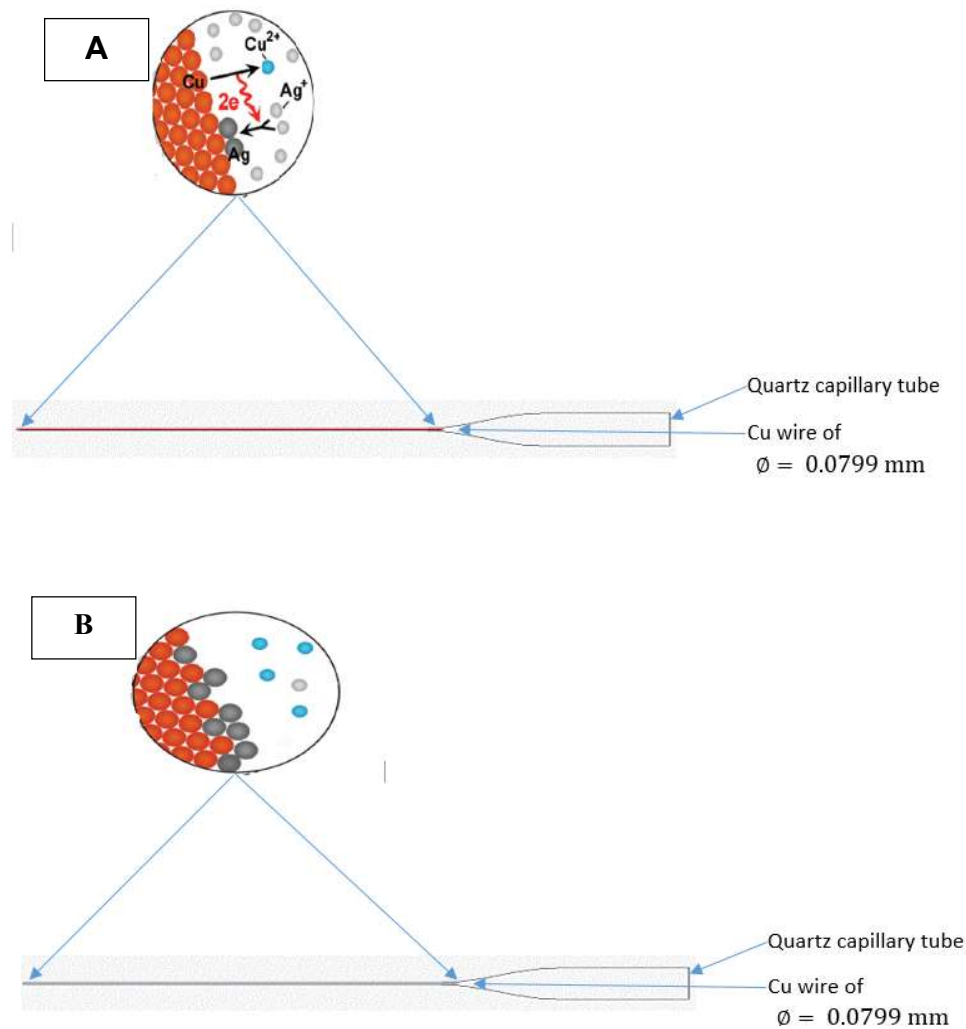


Figure 13 : Schematic of the galvanic replacement reaction in the capillary tube for Ag dendrite formation. (A) Capillary tube with Cu wire immediately after the injection of the AgNO_3 solution. (B) After the galvanic replacement reaction which had proceeded for 5 min.

The electrons from the Cu wire surface can go through the top of Ag atoms, they even can reach to the dendrites tip. The Ag ions could obtain electrons to grow Ag from the tip position. As Ag crystal growth prefer to (111) direction, so they can form single

crystal Ag dendrites. The mechanism of Ag dendrite formation on the top of Cu wire substrate is shown in the Figure 14.

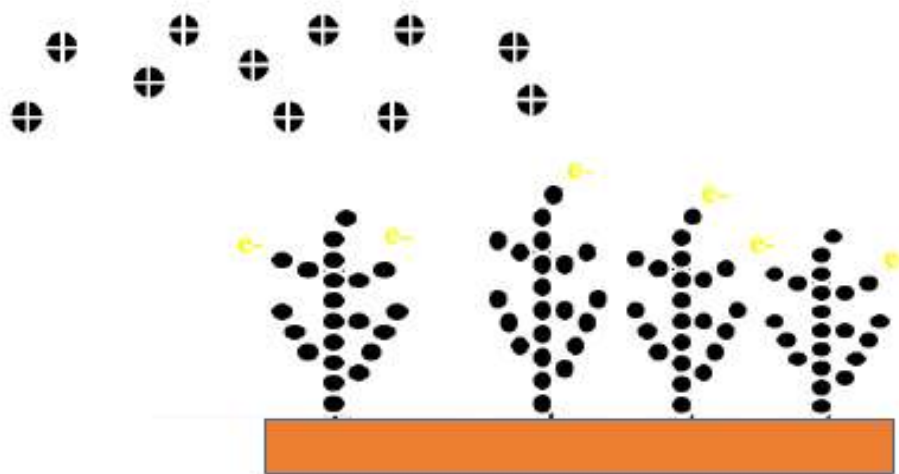


Figure 14: The mechanism for forming Ag Dendrites on the Top of Cu wire substrate.

3.2.2 CHARACTERIZATION

3.2.2.1 SCANNING ELECTRON MICROSCOPY (SEM) AND ENERGY-DISPERSIVE X-RAYS (EDX)

The thin wall capillary quartz tube diagram for Ag nanostructure on the surface of the Cu wire is shown in Figure 15. The SEM and EDX images is shown in Figure 16, for Ag dendrites fabricated at different parts of the capillary tube. It can be seen that at the top part (A) of the capillary tube, the layer of Ag dendrites with symmetrical branches were formed. We can determined that the overall length of the Ag dendrite is almost 12 μm and both the branches and the stems are 30-50 nm in diameter. It is obvious that the silver dendrites are highly symmetrical and all the angles between the stem and branches are almost 60° . In the middle part (B) of the tube we obtain very few, immature and asymmetrical shape Ag dendrite along with large amount of irregular shape Ag

nanostructure on the Cu wire surface. And at the bottom part (C) of the tube, we obtain very small amount and irregular shape Ag nanostructure. The amount of Ag dendrite formation on the surface of the Cu wire decreases from top to bottom of the capillary tube.

The diameter of the capillary tube is very small (i.e. average of 0.2mm) and it decreases from top to bottom. As we know that Ag dendrite formation by GRR process depends on the availability of Ag^+ ions. The top part of the tube has large diameter, so it provides larger volume of the solution, and in turn, a large amount of the Ag^+ ions are available for Ag dendrite formation and the dendrites easily grows on the surface of the Cu wire. This is why we obtain large amount of Ag dendrite at the top part of the capillary tube. As the solution moves down to the middle part, less amount of Ag^+ ions available for the growth of the Ag dendrite because large amount of Ag^+ ions are consumed at the top part. Thus, this affect the size of the dendrite growth and we get small size and asymmetrical shape Ag dendrite at the middle part of the tube. We also obtain large amount irregular shape Ag nanostructure at the middle part due to GRR process, which could not grow into full dendrite structure. At the bottom part of the capillary tube, very small amount of Ag^+ ions are available for GRR process, so the Ag dendritic structure formation is not possible and some irregular shape Ag nanostructures formed. In summary, each time when the AgNO_3 solution is injected in the capillary tube large amount of Ag^+ ions are consumed at the top and very few ions were available as the solution move down the tube.

The composition of the nanostructures is confirmed with EDX at the different part of the capillary tube. At the top of the capillary tube the Ag peak is much higher than Cu which comes from Cu wire substrate, indicating the dendrites are pure Ag. As we move

down of the capillary tube the Ag peak decreases and Cu peak increases indicating that amount of Ag nanostructure formation on the Cu wire decreases.

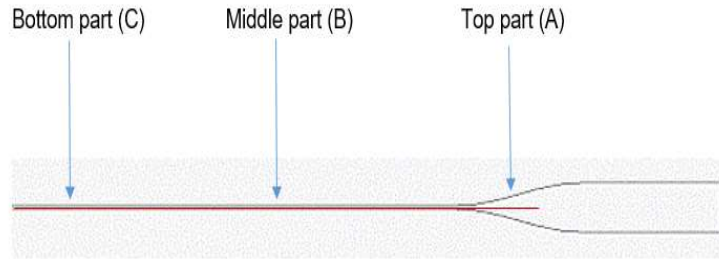
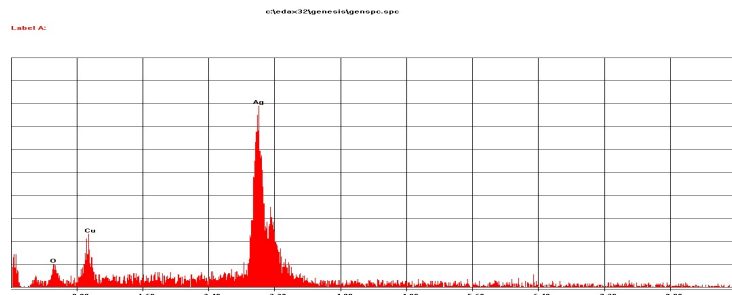
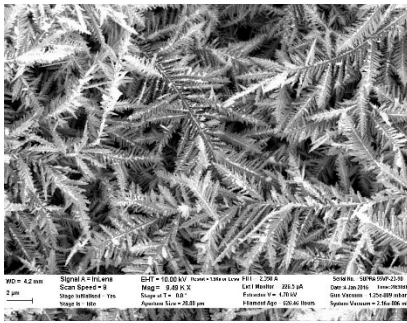
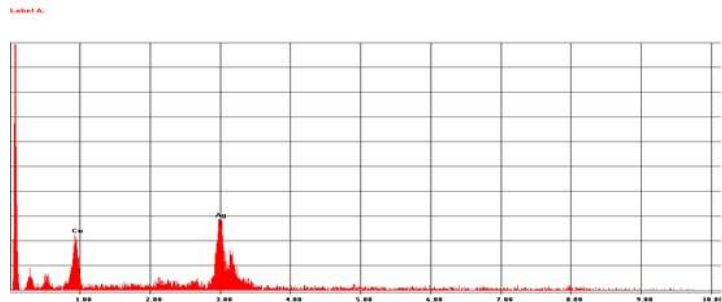
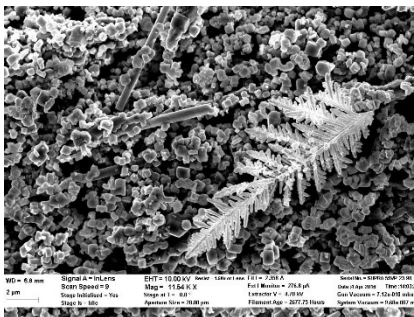


Figure 15 : Thin wall Quartz capillary tube with Ag dendrite formed on the Cu wire

A. Top part



B. Middle part



C. Bottom part

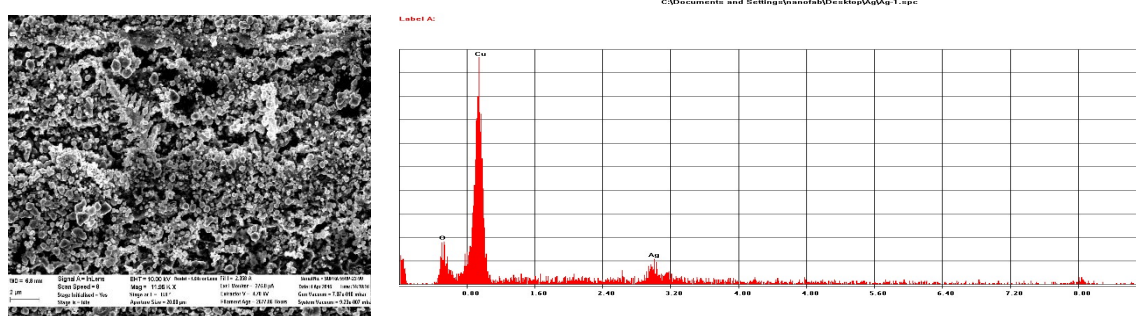


Figure 16: SEM and EDX images of the Ag dendrite formed on the Cu wire surface in the Capillary tube. (A) Top part, (B) Middle part and (C) Bottom part.

3.2.2.2 SERS Results

After we get a large amount of Ag dendrites on the top part of the capillary tube, the 4-MBA aqueous solution with concentration of 1.0×10^{-5} M was injected in the capillary tube to determine the SERS effect. The Raman spectroscopy measurement was conducted using DXR Thermo Fisher Raman microscopy with a 780 nm laser. The signal was collected with 2s of exposure time and laser power is 100 mW.

The Raman spectrum of 4-MBA aqueous solution with concentration of 1.0×10^{-5} M at different part of the capillary tube are shown in the Figure 17, displaying the major vibrational modes of 4-MBA at 1014, 1075, 1139, 1186, 1386, 1587 cm^{-1} , in a good agreement with the reported SERS spectra in the literature [98]. It can be seen that the highest enhancement is obtained at the top part of the capillary tube and lowest enhancement at the bottom part. As Ag dendrite generates a large amount of hot spots for the SERS effect, so at the top part we have highest enhancement. The amount and size of the dendrite decrease with the distance from the top which in turn, decrease the

available hotspots. At the bottom, only irregular shape nanostructures are present, so the lowest enhancement happened at the bottom.

Unlike commonly used SERS measurements where the analyte solution is dropped on the substrate and let the solution dry, all the Raman spectra measurements here were conducted for aqueous solution. Measuring solution has several advantages of the dry form SERS measurements. Solution is highly uniform and easy to obtain reproducible signals; also the measurement obtains accurate structural information of the probe molecules in the solution [98].

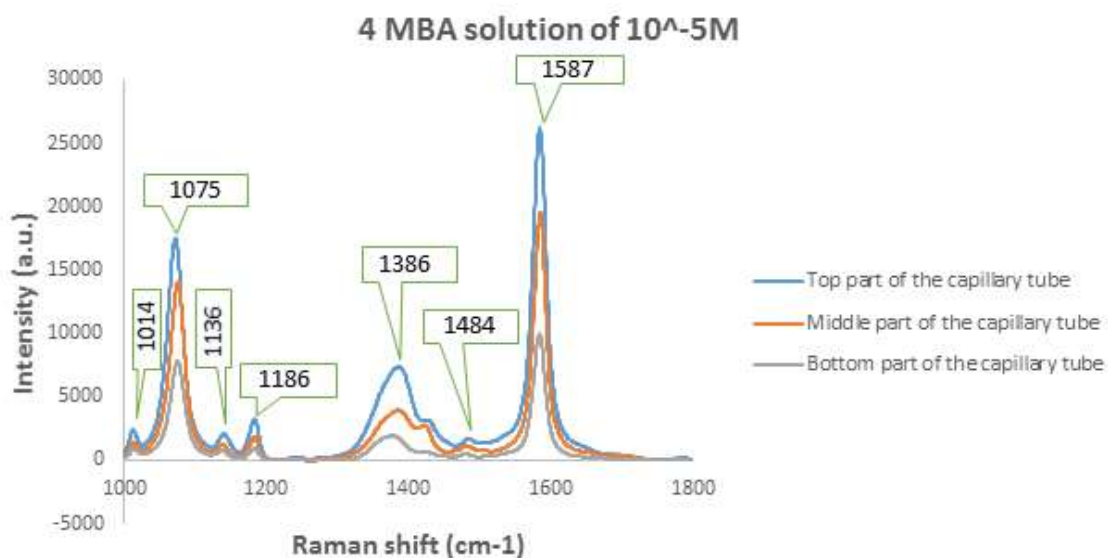


Figure 17: Raman Spectrum of the 4-MBA (1.0×10^{-5} M) aqueous solution on the as-prepared Ag dendrite on the Cu wire in the capillary tube.

Figure 18 depicts the SERS spectra of 4-MBA at different concentrations on the as-synthesized substrates. The detection limit for 4-MBA could be achieved at a concentration as low as 10^{-8} M.

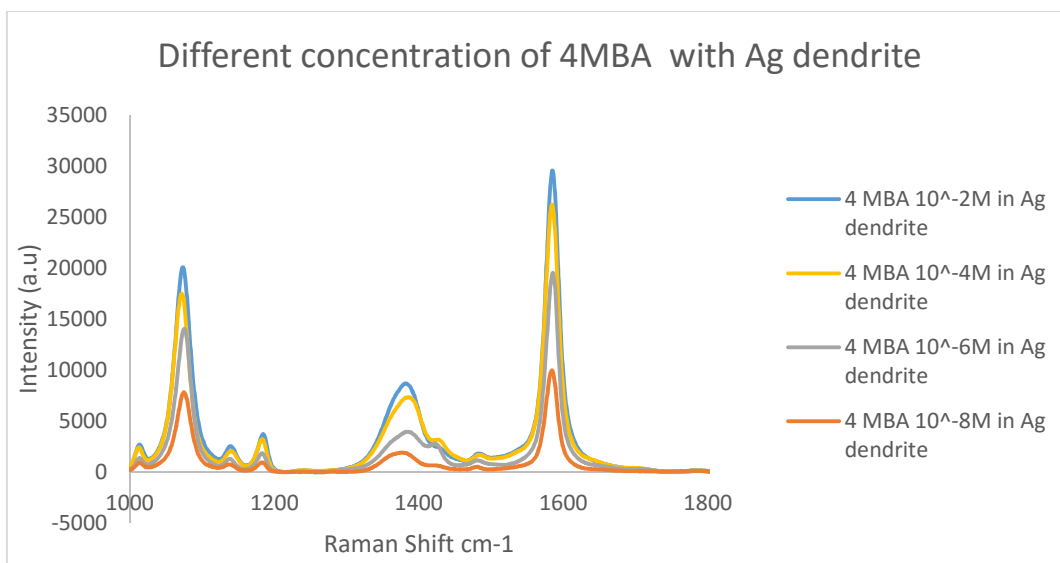


Figure 18: SERS spectra of 4- MBA from concentration from 10^{-2} M till 10^{-8} M in Ag dendrite in the capillary tube.

3.3. Au-Ag DENDRITES IN THE CAPILLARY TUBE

3.3.1 SYNTHESIS

The pre-prepared Ag dendrite on the Cu wire in the capillary tube is used for the fabrication of Au-Ag dendrites. It has been reported in the literature the amount of the Au replacement on Ag dendrite should be of appropriate concentration to get good SERS enhancement [99]. Thus for synthesis of the Au- Ag nanostructure, 25 mM of the HAuCl_4 solution was taken in the 3 ml syringe and injected slowly for 5 min into capillary tube with the pre-prepared Ag dendrite inside. After this process, saturated NaCl solution was injected slowly for 20 minutes into the capillary tube to clean up AgCl byproduct that may have settled on the synthesized nanostructure. Then the sample was cleaned by DI water for 30 mins and dried in air.

3.3.2. CHARACTERIZATION OF Au-Ag NANOSTRUCTURES

3.3.2.1. SCANNING ELECTRON MICROSCOPY (SEM) AND ENERGY-DISPERSIVE X-RAYS (EDX)

(A) Top part of the capillary tube

Figure 19 shows SEM and EDX images of Ag dendrites after replacement of Au at the top part of the capillary tube. As shown in Figure 19a, the dimension of the dendrite does not have any apparent change only small holes are formed on the surface. This indicate that the replacement reaction is taken place on few part of Ag dendrite rather than on entire surface of the Ag dendrite. Thus there is some change in the morphology of the Ag dendrite due to Au atoms replacement. As shown in Figure 19b, the holes can be clearly observed as black spots on the surfaces of some dendrites. This is confirmed from the Figure 19c, which shows the EDX image, the Au peak can be easily identified, even though it is much weaker than the Ag peak.

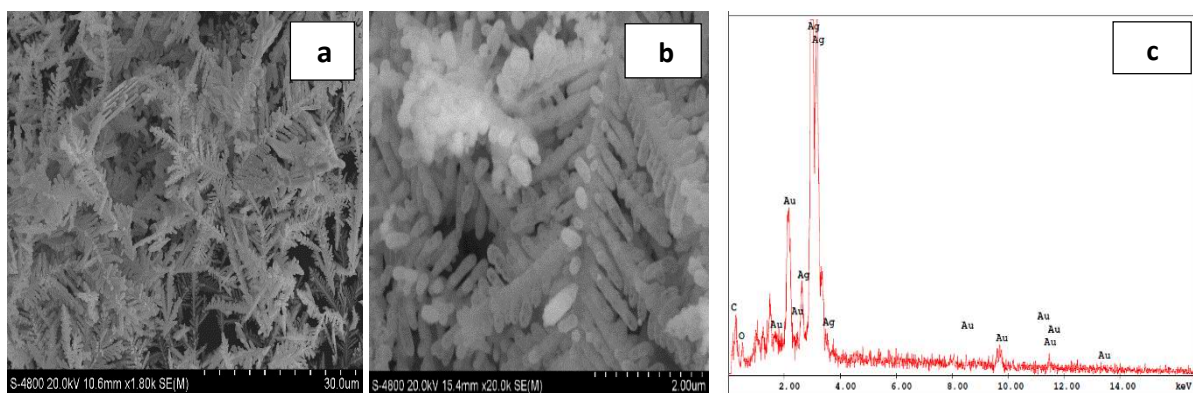


Figure 19: SEM and EDX images of Au-Ag dendrite formed on the Cu wire at the top part of the capillary tube

(B) Middle part of the Capillary tube

Figure 20 shows the SEM and EDX images of the middle part of the capillary tube. In Figure 20a, it can be seen that some immature Ag dendrites are formed with some cuboctahedron particles. As shown in Figure 20b, the magnified image of the dendrite, it is clear that the dendrite formed at the middle part is small in size and asymmetrical in shape due to very few ions are available for the Ag dendrite growth. Figure 20d shows the cuboctahedron shape particles with smooth surface and sharp corners, and with an average edge length of 100 nm. These particles may be formed by dealloying process in the galvanic replacement reaction [97]. Also, small amount of irregular shaped nanostructures are also formed.

The composition is determined with EDX . As shown in Figure 20c, the Ag peak is much higher than the Au peak, indicating that only very small amount of Ag is replaced by Au. The Cu peak in EDX is due to the Cu wire substrate. Figure 20e shows the EDX of cuboctahedron nanoparticle with very small amount of Au

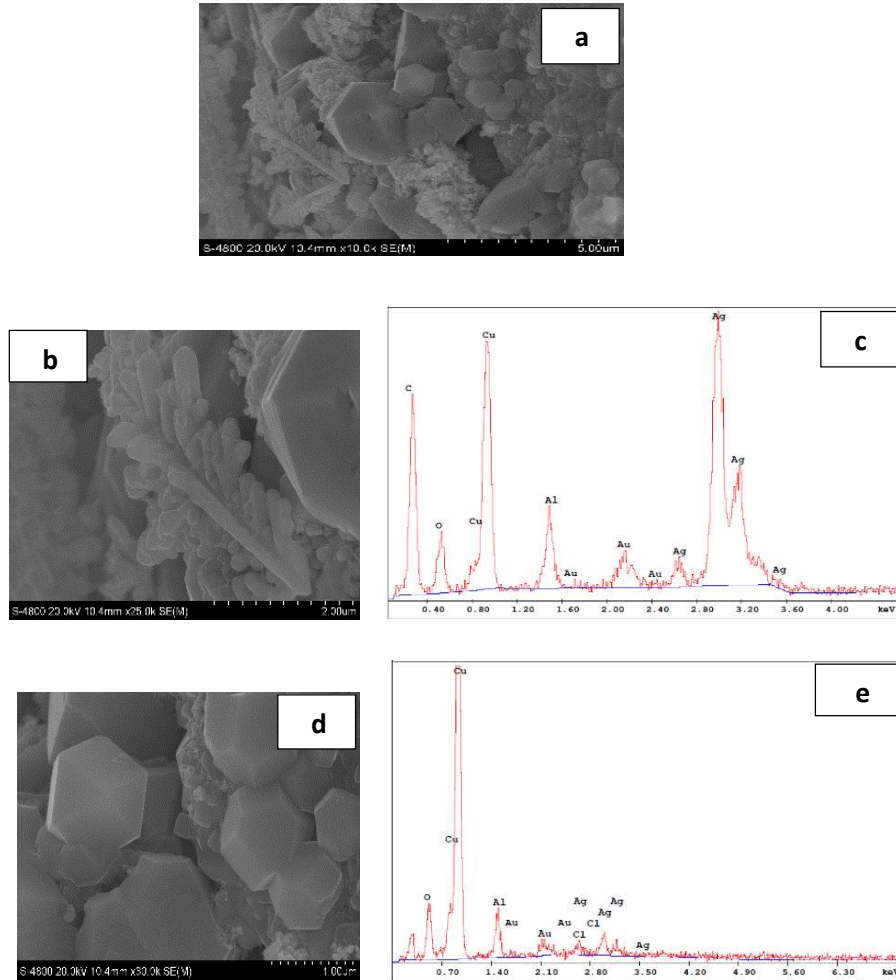


Figure 20: SEM and EDX images of Au-Ag dendrite formed on the Cu wire at the middle part of the capillary tube

C) Bottom part of the capillary tube

Figure 21 shows SEM and EDX image of the nanostructures at the bottom part of the capillary tube. As shown in Figure 21a, only small size of cuboctahedron and irregular shape nanostructure are formed. Figure 21b, the magnified image, shows very few cuboctahedron shape particles are obtained and most of the particles are irregular shape nanostructures. The Figure 23c, shows the EDX image which determines that negligible amount of Au is obtained.

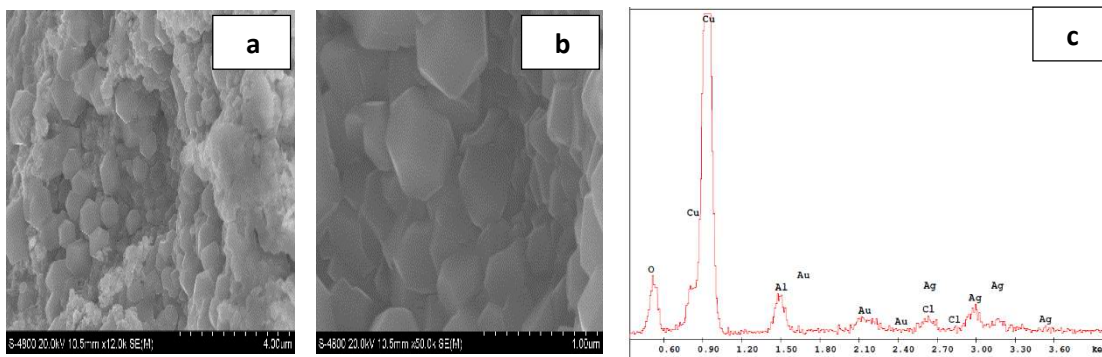


Figure 21: SEM and EDX images of Au-Ag dendrite formed on the Cu wire at the bottom part of the capillary tube

3.3.2.2 SERS RESULTS

After we get a large area of Au-Ag bimetallic dendrites on the top surface of the Cu wire substrate in the capillary tube, the 4-MBA aqueous solution with concentration of 1.0×10^{-5} M was injected in the capillary tube to determine the SERS effect.

The Raman spectra of 4-MBA aqueous solution with concentration of 1.0×10^{-5} M at different part of the capillary tube (different Au-Ag nanostructures) are shown in Figure 22, displaying the major vibrational modes of 4-MBA at 1014, 1075, 1139, 1186, 1386, 1587 cm^{-1} . It can be seen again that highest enhancement is obtained at the top part of the capillary tube and lowest enhancement at the bottom part. As dendrite generates huge amount of hot spots for the SERS effect, so at the top part we have highest enhancement. It decreases as we move down of the tube due to decreases in amount and size of the dendrite. At the bottom only irregular shape nanostructure are present, so we obtain lowest enhancement. Figure 23 depicts the SERS spectra of 4-MBA at different concentrations on the as-synthesized Ag-Au substrates. The detection limit for 4-MBA could be achieved at a concentration as low as 10^{-12} M.

This extremely high SERS effect shown by Au-Ag bimetallic nano-dendrites is related to several factors. First, dendrite structure along with the surfaces of bimetals provides more possibilities for molecules to deposit on the boundaries between Ag and Au domains. Two close metallic surfaces can enhance the electromagnetic (EM) field around molecules absorbed between them, which leads to large SERS enhancement [93]. Second, adequate amounts of Au in a homogeneous alloy (solid solution) may intrinsically enhance the SERS activity. However, the most important reason may be related to the corresponding morphological change of the underlying Ag dendrite occurred during the GRR process, pores formed where Ag is depleted.

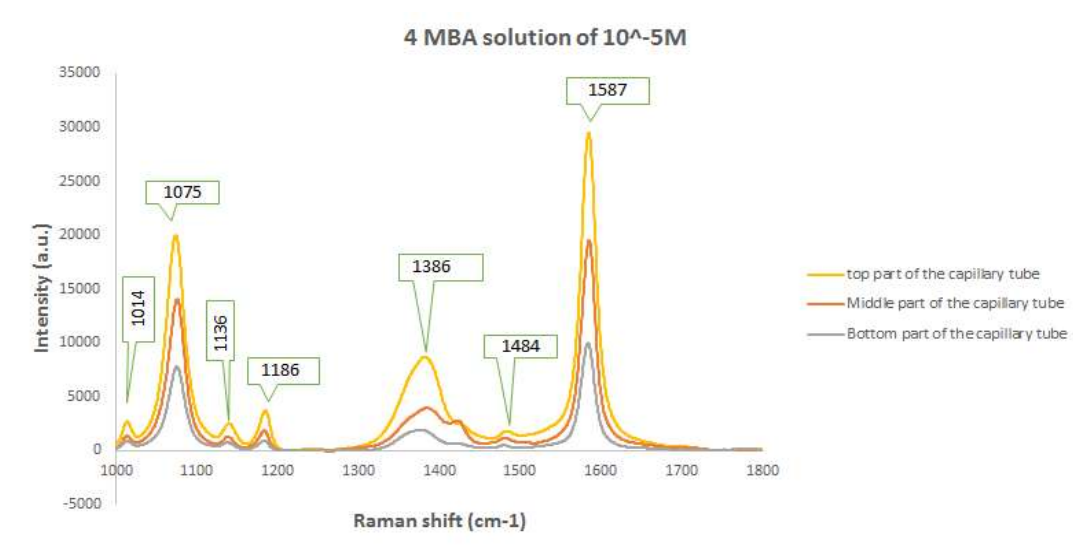


Figure 22: Raman Spectrum of the 4 MBA (1.0×10^{-5} M) aqueous solution on the as prepared Au-Ag nanostructure on the Cu wire in the capillary tube.

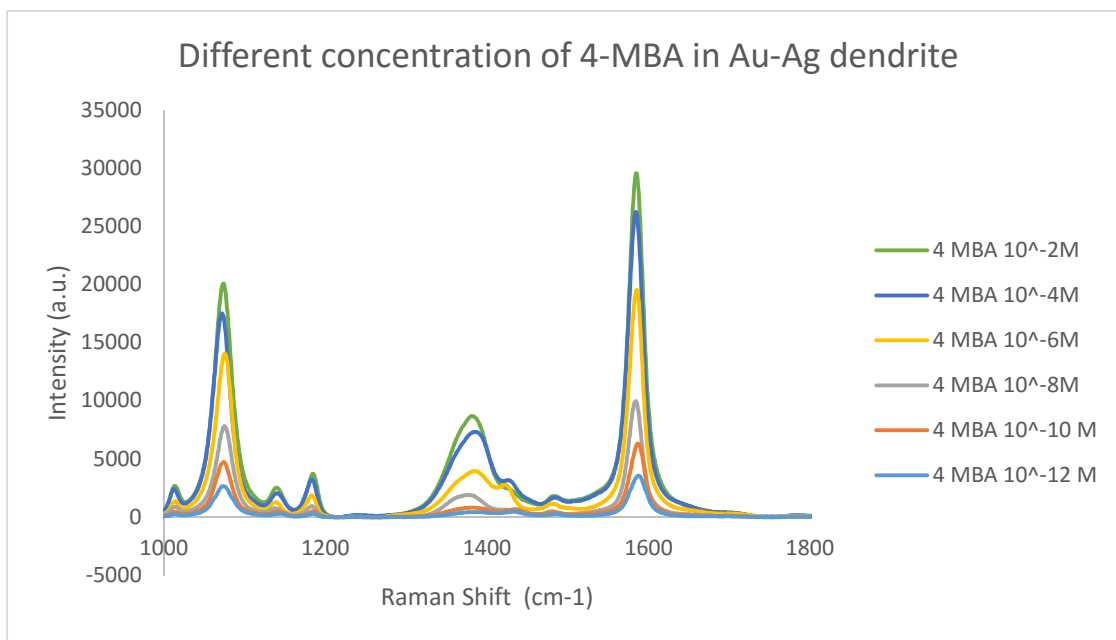


Figure 23: SERS spectra of 4- MBA from concentration from 10^{-2} M till 10^{-12} M is acquired from Au-Ag dendrite in the capillary tube.

3.3.3 MECHANISM OF FORMING Au-Ag NANOSTRUCTURES

The Au-Ag nanostructure is obtained by galvanic replacement reaction (GRR). Since the standard electrode potential of $\text{AuCl}_4^- / \text{Au}$ pair (0.99V vs SHE) is higher than that of AgCl/Ag pair (0.22 V vs SHE), silver undergoes GRR with AuCl_4^- ions [93].

The synthesis mechanism of Au-Ag nanostructure has been analyzed from the schematic as shown in Figure 24. When HAuCl_4 solution is injected in the capillary tube of pre-prepared Ag dendrite. The galvanic replacement reaction initiate immediately at the site of high surface energy locations (for example defects, stacking fault or steps). The Ag atom undergoes oxidation into Ag^+ ions and this ions dissolved into the solution and generating small holes on the surface of the nanoparticle. At the same time AuCl_4^- ions are captured by the electrons that are migrated to the surface of the nanoparticles to

form Au atoms by reduction reaction. The Au atoms tends to deposited epitaxially on the surface of the Ag nanoparticles. The initial GRR process deposits Au nuclei on Ag dendrite (scheme a). As the nucleation progress the nuclei of gold turns into different size of flakes further in the process. At the same time dissolution of the Ag takes place, thus the Ag atoms are depleted which leads to formation of the pores in Ag dendrite (Scheme b). The Au atoms continuously covered the Ag dendrite surface forming a layer of Au on the surface of Ag dendrite and subsequently concentration of AuCl_4^- gradually decreases, both of this leads to slow down the GRR. Because of this the nucleation is terminated (Scheme c). In the end porous bimetallic nanostructure is generated from the cavities between Au flakes and pores between the more and more depleted original Ag dendrite (Scheme d). The Au flakes formed on the surface basically hide the Ag pores [93].

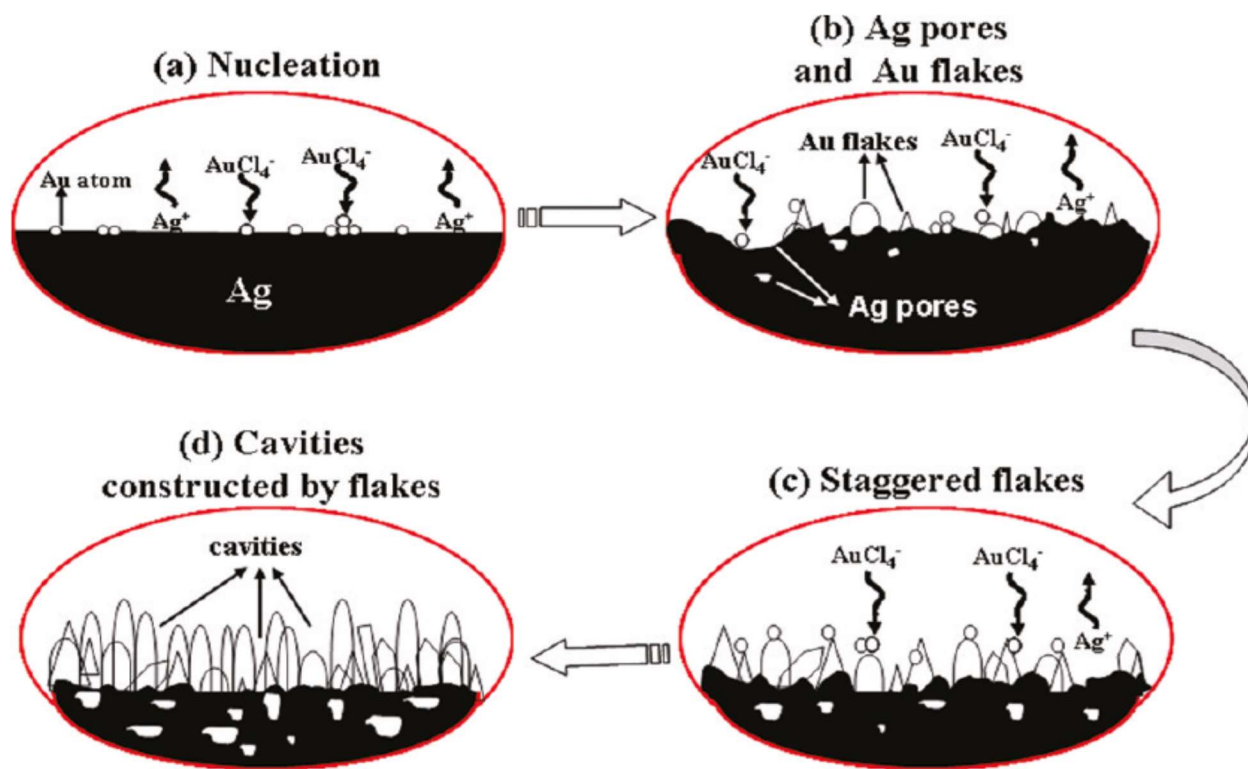


Figure 24 Schematic diagram of Au- Ag nanostructure synthesis by GRR

The equation involved in this galvanic replacement reaction can be summarized as follows:



3.4 Pd-Ag DENDRITES IN THE CAPILLARY TUBE

3.4.1 SYNTHESIS

The pre-prepared Ag dendrite in the capillary tube is used for the fabrication of Pd-Ag dendrites. It has been reported in the literature that the amount of the Pd replacement on Ag dendrite need to be an appropriate concentration to get good SERS enhancement [96]. Thus for synthesis of the Pd-Ag nanostructure, 25 mM of the PdCl₄ solution was taken in the 3 ml syringe and injected slowly for 5 min into capillary tube with the pre-prepared Ag dendrite inside. After this process, saturated NaCl solution was injected slowly for 20 minutes into the capillary tube to clean up AgCl byproduct that may have settled on the synthesized nanostructure. Then the sample was cleaned by DI water for 30 mins and dried in air

3.4.2 CHARACTERIZATION OF Pd-Ag NANOSTRUCTURES

3.4.2.1. SCANNING ELECTRON MICROSCOPY (SEM) AND ENERGY-DISPERSIVE X-RAYS (EDX)

A. Top part of the capillary tube

Figure 25 shows SEM and EDX images of Ag dendrites after replacement of Pd atoms at the top part of the capillary tube. As shown in Figure 25a, large amount of Pd

replaced Ag dendrite are formed. Figure 25b shows the magnified image of Pd replaced Ag dendrite. The overall dendrite structure remains the same but there is some change in shape and size of the dendrites. The previously sharp tip of the Ag dendrites are now become more spherical in shape and the dendrite are now covered with a new, rough surface of the Pd granules. This indicates that the replacement reaction is taken place on the Ag dendrite surface and the morphology of the entire Ag dendrite changes due to Pd atom replacement. This is confirmed from the Figure 25c, which shows the EDX image, the Pd peak can be easily identified, even though it is much weaker than the Ag peak.

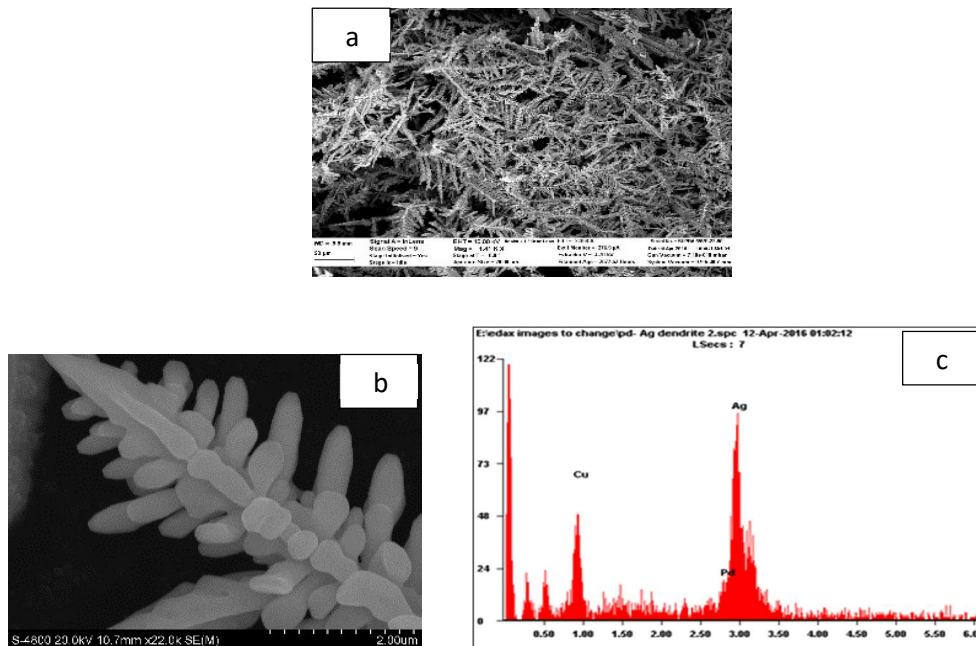


Figure 25: SEM and EDX images of Pd-Ag dendrite formed on the Cu wire at the top part of the capillary tube.

B. Middle part of the capillary tube

Figure 26 shows the SEM and EDX images of the middle part of the capillary tube. In Figure 26a, it can be seen that very few and immature dendrites are formed with some

nanocube shaped particles. Figure 26b shows the magnified image of the dendrite, it is clear that the dendrite formed at the middle part is small and immature due to the few amount of Ag^+ ions available at the middle part of the tube.

The composition is confirmed by the EDX images. As shown in Figure 26c, the EDX image of the Ag dendrite, the Ag peak are much higher than the Pd peak, indicating that very small amount of Ag is replaced by Pd.

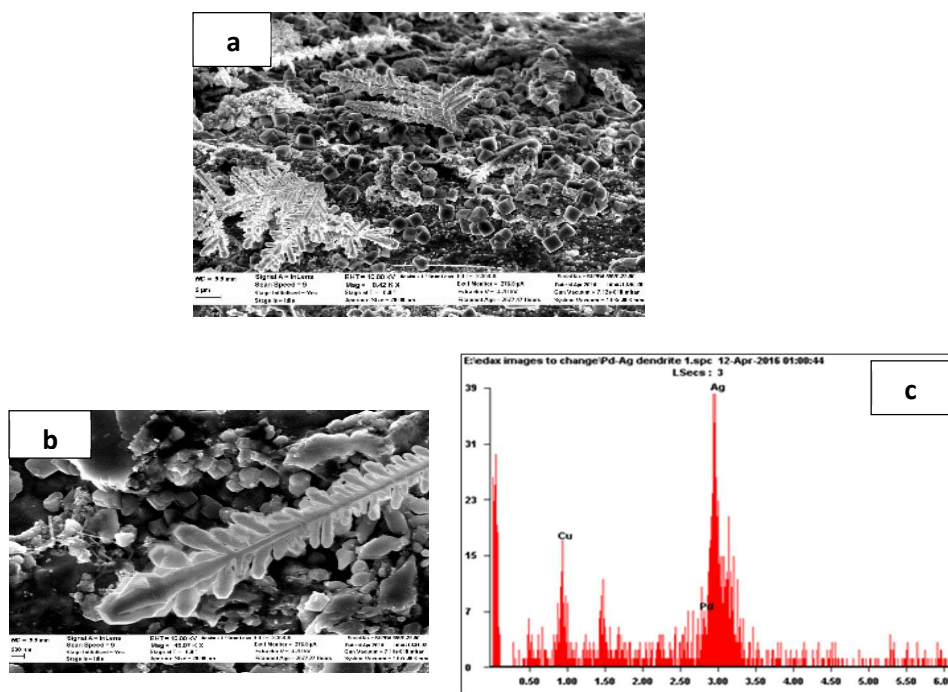


Figure 26: SEM and EDX images of Pd-Ag dendrite formed on the Cu wire at the middle part of the capillary tube

C. Bottom part of the capillary tube

Figure 27, shows SEM and EDX images of the bottom part of the capillary tube. As shown in Figure 27a, at the bottom part only few nanocube shaped and some irregular shaped nanostructures are formed. Figure 27b, the magnified image, shows the nanocubic shape particles with smooth surface and sharp corners, and with an

average edge length of 100 nm along with most of the irregular shape nanostructures. The Figure 27c, shows the EDX image of the broken nanocube which determines that the nanocube consists of negligible amount of Pd.

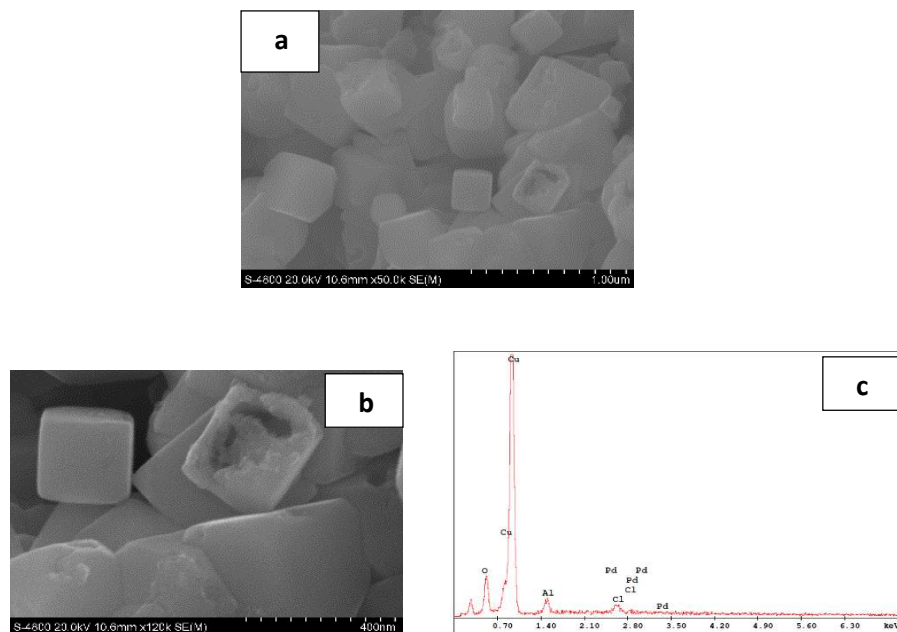


Figure 27: SEM and EDX images of Pd-Ag nanostructure formed on the Cu wire at the bottom part of the capillary tube.

3.4.2.2 SERS RESULTS

After we get a large area of Pd-Ag bimetallic dendrites on the top part in the capillary tube, the 4-MBA aqueous solution with concentration of 1.0×10^{-5} M was injected in the capillary tube to determine the SERS effect.

The Raman spectra of 4-MBA aqueous solution with concentration of 1.0×10^{-5} M at different part of the capillary tube displayed the major vibrational modes of 4-MBA at 1014, 1075, 1139, 1186, 1386, 1587 cm^{-1} as shown in the Figure 28. From the Raman

spectra we determine that highest enhancement is obtained at the top part of the capillary tube and lowest enhancement at the bottom part. Figure 29 depicts the SERS spectra of 4 MBA at different concentrations on the as-synthesized substrates. The detection limit for 4 MBA could be achieved at a concentration as low as 10^{-13} M.

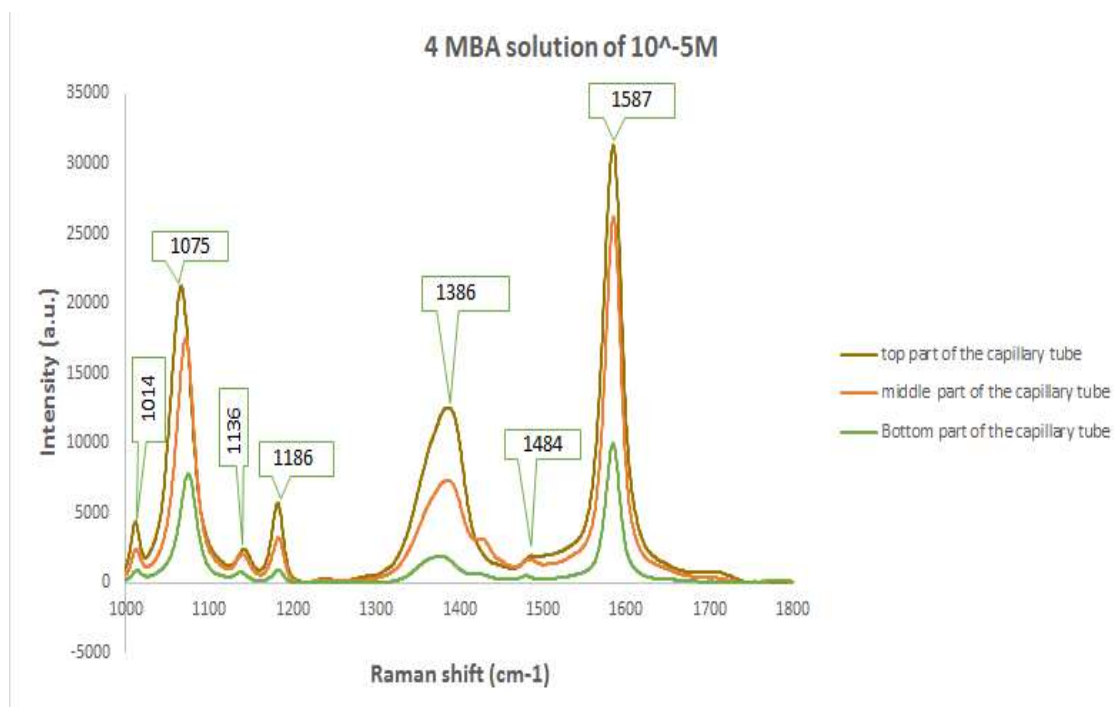


Figure 28 : Raman Spectrum of the 4 MBA (1.0×10^{-5} M) aqueous solution on the as prepared Pd-Ag dendrite on the Cu wire in the capillary tube.

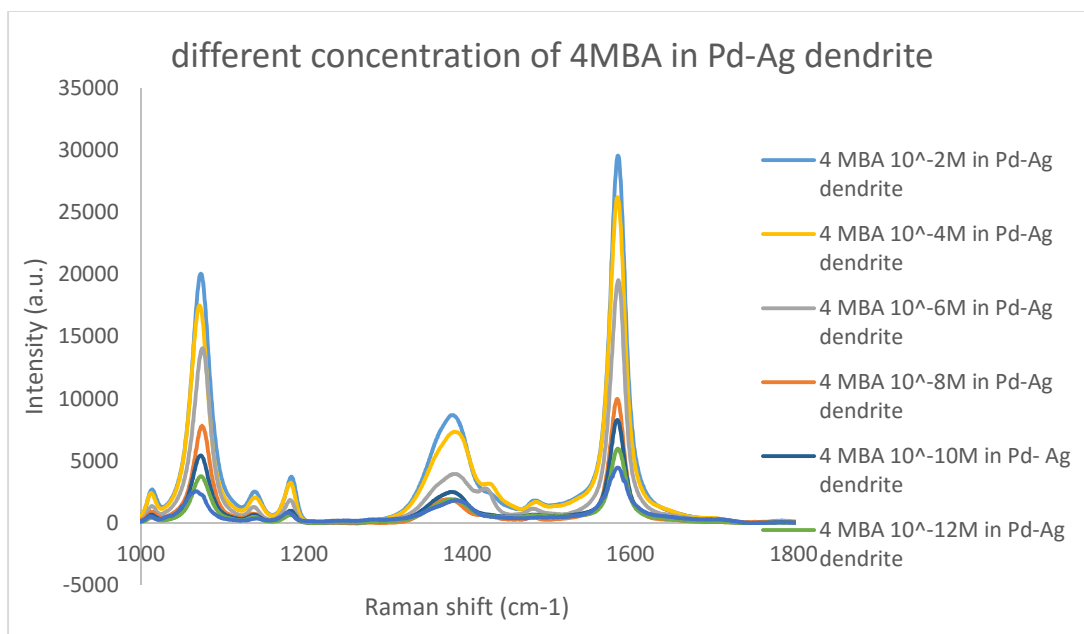


Figure 29: SERS spectra of 4- MBA from concentration from 10^{-2} M till 10^{-13} M in acquired from Pd-Ag dendrite in the capillary tube.

3.4.3 MECHANISM OF FORMATION OF Pd - Ag NANOSTRUCTURE.

The Pd - Ag nanostructure is obtained by galvanic replacement reaction (GRR). Since the standard reduction potential of $\text{PdCl}_4^{2-} / \text{Pd}$ pair (0.83 V vs SHE) is higher than 0.61V than that of AgCl/Ag pair (0.22 V vs SHE), Silver undergoes GRR with PdCl_4^{2-} ions [96].

The equation involved in this galvanic replacement reaction can be summarized as follows:



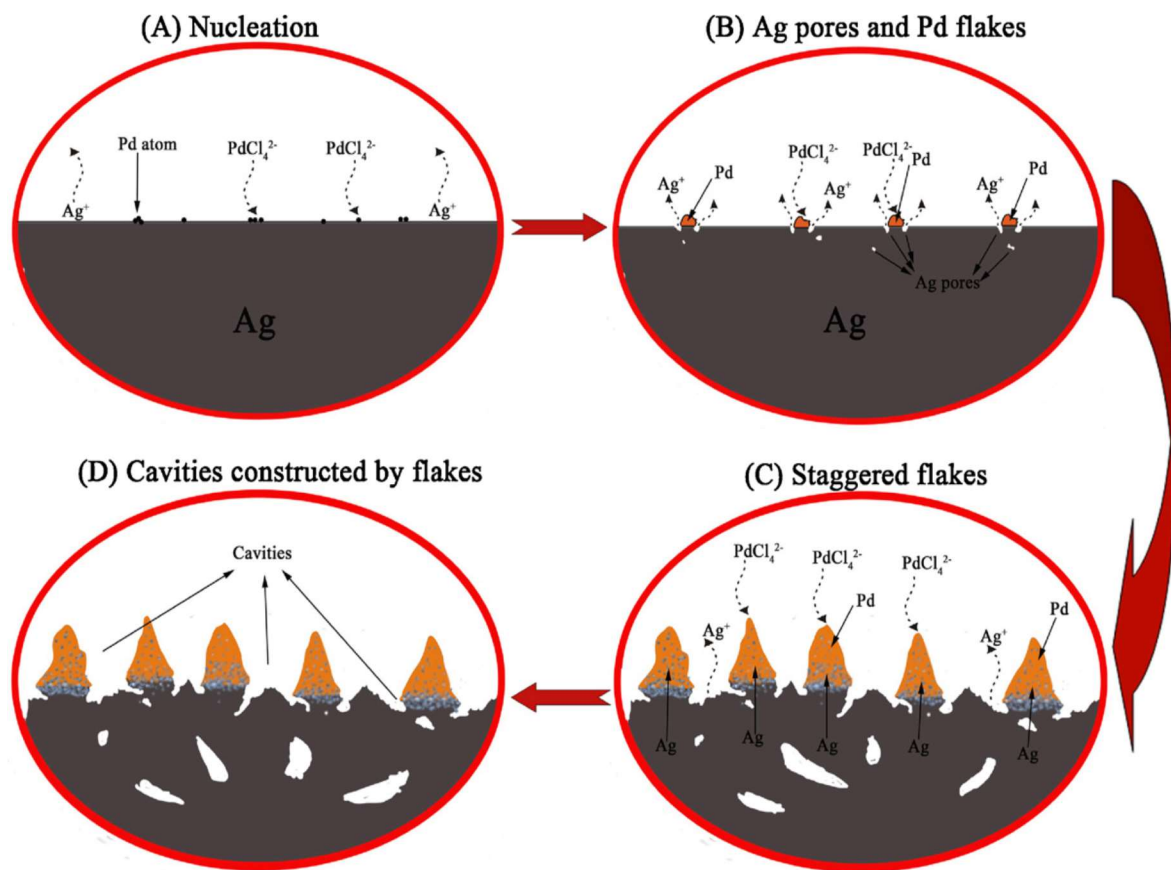


Figure 30: Schematic diagram of Pd- Ag nanostructure synthesis by GRR

CHAPTER 4

CONCLUSION

In summary, we synthesized the 3D SERS substrates in thin wall quartz capillary tube on Cu wire by GRR. These 3D SERS substrates consists of Ag dendrite, Au-Ag and Pd-Ag bimetallic nanostructures. This 3D hierarchical nanostructure obtained in the capillary tube provides high-density and uniform distribution of hotspots along the three-dimension directions and also provides large surface area for absorbing more probe molecules. Thus they lead to have extremely high SERS enhancement and can detect low concentration molecules. So these 3D fabricated substrate was employed to detect the 4-MBA solution to the detection limit down to 10^{-13} M.

In the synthesis process, Cu wire which is used as substrate was inserted in the thin walled quartz capillary tube and then AgNO_3 was injected into the tube to form Ag dendrite on the Cu wire substrate. This pre-prepared dendrite was used to prepare bimetallic nanostructures of Au-Ag and Pd-Ag by injecting chlorauric acid (HAuCl_4) and palladium chloride (PdCl_4) into the tube, respectively. The 3D substrate obtained compromised of dendritic structure only at the top part of the capillary tube. The middle part consist of few dendritic structure and lot of irregular shape nanostructure. The bottom part of the tube consist only irregular shaped nanostructure. This is due the reason that the average diameter of the tube was too small (i.e. 0.2mm) and it decreases from top to bottom of the tube. Thus the top part of the tube has large diameter, so it provides larger volume of the solution, and in turn, a large amount of the ions are available for Ag dendrite formation and the dendrites easily grows on the surface of the Cu wire. As the solution moves down to the middle part, less amount of ions are available for the growth of the Ag

dendrite because large amount of Ag^+ ions are consumed at the top part. Thus, this affect the size of the dendrite growth and we get small size and asymmetrical shape of dendrite, along with large amount irregular shape nanostructure at the middle part due to GRR process, which could not grow into full dendrite structure. At the bottom part of the capillary tube, very small amount of ions are available for GRR process, so the dendritic structure formation is not possible and some irregular shape Ag nanostructures formed. In summary, each time when the solution is injected in the capillary tube large amount of ions are consumed at the top and very few ions were available as the solution move down the tube.

The GRR process leads to the replacement of Ag atoms by Au and Pd which causes corresponding morphological change of the underlying Ag dendrite. The GRR leaves pores where Ag is depleted.

For SERS results 4-MBA aqueous solution of various concentration was used. The results indicated that Ag dendrite can detect only till 10^{-8} M 4-MBA solution as compared to Au-Ag and Pd-Ag can detect till 10^{-13} M and 10^{-12} M respectively. Thus due to morphology and structural change in the dendritic structure of Pd-Ag and Au-Ag bimetallic nanostructure it can detect low concentration of the molecules as compared to the Ag dendrite substrate. The Pd-Ag nano-dendrites can detect 4 MBA aqueous solution till concentration of 10^{-13} M, while Au-Ag nano-dendrites can detect till concentration of 10^{-12} M. This may be due to the morphological and structural changes generated by GRR process in Pd- Ag. The Pd-Ag nano-dendrites surface has become rough due the Pd replacement on the surface. Thus may supply more optimized pores on the Ag depletion due to the appropriate concentration of solution added for appropriate reaction time. On

the other hand in the Au-Ag nano-dendrite there is not a lot of change in the morphology. Only on some part of the dendrite surface, small holes are formed. So this may be due to inadequate concentration of the solution added or due to the inappropriate reaction time.

Further work is expected to be done yet to obtain to uniform dendritic structure in overall interior of the capillary. This could be achieved by using more larger and uniform diameter of the tube. Reaction conditions can be varied by changing the concentration of the solution used and also by changing the reaction time.

REFERENCES

1. Yu, J. and X. Zhou, *Synthesis of Dendritic Silver Nanoparticles and Their Applications as SERS Substrates*. Advances in Materials Science and Engineering, 2013. **2013**: p. 1-4.
2. Cong, F.-Z., et al., *A facile synthesis of branched silver nanowire structures and its applications in surface-enhanced Raman scattering*. Frontiers of Physics, 2012. **7**(5): p. 521-526.
3. Huang, J., et al., *3D Silver Nanoparticles Decorated Zinc Oxide/Silicon Heterostructured Nanomace Arrays as High-Performance Surface-Enhanced Raman Scattering Substrates*. ACS Applied Materials & Interfaces, 2015. **7**(10): p. 5725-5735.
4. Cai, W.Y., et al., *Facile fabrication of leafy spikes-like silver dendrite crystals for SERS substrate*. Materials Research Bulletin, 2013. **48**(10): p. 4125-4133.
5. Xie, S.P., et al., *Fast Growth Synthesis of Silver Dendrite Crystals Assisted by Sulfate Ion and Its Application for Surface-Enhanced Raman Scattering*. Journal of Physical Chemistry C, 2011. **115**(20): p. 9943-9951.
6. Cong, F.Z., et al., *A facile synthesis of branched silver nanowire structures and its applications in surface-enhanced Raman scattering*. Frontiers of Physics, 2012. **7**(5): p. 521-526.
7. Chen, H., et al., *Investigation of the synthesis, SERS performance and application in glucose sensing of hierarchical 3D silver nanostructures*. New Journal of Chemistry, 2014. **38**(8): p. 3907-3916.
8. Xia, Y.Y., et al., *Facile fabrication of hierarchically flowerlike Ag microstructure for SERS application*. Journal of Materials Science, 2014. **49**(7): p. 2781-2786.
9. Li, Y., et al., *Lipid and lipid oxidation analysis using surface enhanced Raman spectroscopy (SERS) coupled with silver dendrites*. Food Research International, 2014. **58**: p. 1-6.
10. Xia, Y.Y. and J.M. Wang, *Hierarchical silver nanodendrites: One-step preparation and application for SERS*. Materials Chemistry and Physics, 2011. **125**(1-2): p. 267-270.
11. Zhang, W., et al., *Facile, template-free synthesis of silver nanodendrites with high catalytic activity for the reduction of p-nitrophenol*. Journal of Hazardous Materials, 2012. **217**: p. 36-42.
12. Gao, P., et al., *A simple template method for hierarchical dendrites of silver nanorods and their applications in catalysis*. Materials Research Bulletin, 2008. **43**(3): p. 531-538.

13. Rashid, M.H. and T.K. Mandal, *Synthesis and catalytic application of nanostructured silver Dendrites*. Journal of Physical Chemistry C, 2007. **111**(45): p. 16750-16760.
14. Han, S.H., L.S. Park, and J.S. Lee, *Hierarchically branched silver nanostructures (HBAgNSs) as surface plasmon regulating platforms for multiplexed colorimetric DNA detection*. Journal of Materials Chemistry, 2012. **22**(38): p. 20223-20231.
15. Fu, J.J., W.C. Ye, and C.M. Wang, *Facile synthesis of Ag dendrites on Al foil via galvanic replacement reaction with Ag(NH₃)₂ Cl for ultrasensitive SERS detecting of biomolecules*. Materials Chemistry and Physics, 2013. **141**(1): p. 107-113.
16. Hu, Y.W., et al., *Superhydrophobicity and surface enhanced Raman scattering activity of dendritic silver layers*. Thin Solid Films, 2010. **519**(4): p. 1314-1318.
17. Gu, C.D. and T.Y. Zhang, *Electrochemical Synthesis of Silver Polyhedrons and Dendritic Films with Superhydrophobic Surfaces*. Langmuir, 2008. **24**(20): p. 12010-12016.
18. Huang, J., et al., *Highly Catalytic Pd-Ag Bimetallic Dendrites*. The Journal of Physical Chemistry C, 2010. **114**(35): p. 15005-15010.
19. Jiang, R., *Plasmonic nanostructures for surface-enhanced Raman spectroscopy*. 2014.
20. Wokaun, A., J.P. Gordon, and P.F. Liao, *Radiation Damping in Surface-Enhanced Raman Scattering*. Physical Review Letters, 1982. **48**(14): p. 957-960.
21. Bell, S.E.J. and N.M.S. Sirimuthu, *Surface-Enhanced Raman Spectroscopy (SERS) for Sub-Micromolar Detection of DNA/RNA Mononucleotides*. Journal of the American Chemical Society, 2006. **128**(49): p. 15580-15581.
22. Doering, W.E., et al., *SERS as a Foundation for Nanoscale, Optically Detected Biological Labels*. Advanced Materials, 2007. **19**(20): p. 3100-3108.
23. Schatz, G.C., M.A. Young, and R.P. Duyne, *Electromagnetic Mechanism of SERS*, in *Surface-Enhanced Raman Scattering: Physics and Applications*, K. Kneipp, M. Moskovits, and H. Kneipp, Editors. 2006, Springer Berlin Heidelberg: Berlin, Heidelberg. p. 19-45.
24. Fievet, F., J.P. Lagier, and M. Figlarz, *Preparing Monodisperse Metal Powders in Micrometer and Submicrometer Sizes by the Polyol Process*. MRS Bulletin, 1989. **14**(12): p. 29-34.
25. Marinakos, S.M., S. Chen, and A. Chilkoti, *Plasmonic Detection of a Model Analyte in Serum by a Gold Nanorod Sensor*. Analytical Chemistry, 2007. **79**(14): p. 5278-5283.
26. <pd on ag dendrite paper.pdf>.
27. Creighton, J.A., *Contributions to the early development of surface-enhanced Raman spectroscopy*. Notes and Records, 2010. **64**(2): p. 175-183.

28. Ahmed, I., et al., *Photocatalytic synthesis of silver dendrites using electrostatic hybrid films of porphyrin-polyoxometalate*. Applied Catalysis a-General, 2012. **447**: p. 89-99.
29. Rycenga, M., et al., *Controlling the Synthesis and Assembly of Silver Nanostructures for Plasmonic Applications*. Chemical Reviews, 2011. **111**(6): p. 3669-3712.
30. Bian, J.C., et al., *Reproducible and recyclable SERS substrates: Flower-like Ag structures with concave surfaces formed by electrodeposition*. Applied Surface Science, 2015. **333**: p. 126-133.
31. Rashid, M.H. and T.K. Mandal, *Synthesis and Catalytic Application of Nanostructured Silver Dendrites*. The Journal of Physical Chemistry C, 2007. **111**(45): p. 16750-16760.
32. Qin, X., et al., *Preparation of Dendritic Nanostructures of Silver and Their Characterization for Electroreduction*. Langmuir, 2012. **28**(11): p. 5218-5226.
33. Mandke, M.V., S.H. Han, and H.M. Pathan, *Growth of silver dendritic nanostructures via electrochemical route (vol 14, pg 8734, 2012)*. Crystengcomm, 2012. **14**(24): p. 8734-8734.
34. Sivasubramanian, R. and M.V. Sangaranarayanan, *A facile formation of silver dendrites on indium tin oxide surfaces using electrodeposition and amperometric sensing of hydrazine*. Sensors and Actuators B-Chemical, 2015. **213**: p. 92-101.
35. Sharma, D.K., et al., *The facile formation of silver dendritic structures in the absence of surfactants and their electrochemical and SERS properties*. Colloids and Surfaces a-Physicochemical and Engineering Aspects, 2011. **386**(1-3): p. 98-106.
36. Chu, J., et al., *A highly-ordered and uniform sunflower-like dendritic silver nanocomplex array as reproducible SERS substrate*. Rsc Advances, 2015. **5**(5): p. 3860-3867.
37. Sawangphruk, M., et al., *Silver nanodendrite modified graphene rotating disk electrode for nonenzymatic hydrogen peroxide detection*. Carbon, 2014. **70**: p. 287-294.
38. Fu, L., et al., *Carbon nanotube and graphene oxide directed electrochemical synthesis of silver dendrites*. Rsc Advances, 2014. **4**(75): p. 39645-39650.
39. Yang, Z., et al., *Electrodepositing Ag nanodendrites on layered double hydroxides modified glassy carbon electrode: Novel hierarchical structure for hydrogen peroxide detection*. Electrochimica Acta, 2013. **90**: p. 400-407.
40. Hu, J.F., et al., *3D Dendritic Nanostructure of Silver-Array: Preparation, Growth Mechanism and Application in Nitrate Sensor*. Electroanalysis, 2013. **25**(2): p. 546-556.
41. Guadagnini, L., B. Ballarin, and D. Tonelli, *Dendritic silver nanostructures obtained via one-step electrosynthesis: effect of nonanesulfonic acid and polyvinylpyrrolidone as*

- additives on the analytical performance for hydrogen peroxide sensing.* Journal of Nanoparticle Research, 2013. **15**(10).
42. Bian, J.C., et al., *Electrodeposition of hierarchical Ag nanostructures on ITO glass for reproducible and sensitive SERS application.* Applied Surface Science, 2012. **258**(17): p. 6632-6636.
 43. Bian, J.C., et al., *Double-potentiostatic electrodeposition of Ag nanoflowers on ITO glass for reproducible surface-enhanced (resonance) Raman scattering application.* Electrochimica Acta, 2012. **67**: p. 12-17.
 44. Qin, X., et al., *Synthesis of dendritic silver nanostructures and their application in hydrogen peroxide electroreduction.* Electrochimica Acta, 2011. **56**(9): p. 3170-3174.
 45. Rezaei, B. and S. Damiri, *Electrodeposited silver nanodendrites electrode with strongly enhanced electrocatalytic activity.* Talanta, 2010. **83**(1): p. 197-204.
 46. Zhang, J.P., C.S. Day, and D.L. Carroll, *Controlled growth of novel hyper-branched nanostructures in nanoporous alumina membrane.* Chemical Communications, 2009(45): p. 6937-6939.
 47. Jiang, Z.Y., Y. Lin, and Z.X. Xie, *Structural investigations and growth mechanism of well-defined Ag dendrites prepared by conventional redox displacement.* Materials Chemistry and Physics, 2012. **134**(2-3): p. 762-767.
 48. Ding, H.P., et al., *Silver dendritic nanostructures formed at the solid/liquid interface via electroless deposition.* Colloids and Surfaces a-Physicochemical and Engineering Aspects, 2010. **353**(2-3): p. 166-171.
 49. Fang, J., et al., *Dendritic Silver Nanostructure Growth and Evolution in Replacement Reaction.* Crystal Growth & Design, 2007. **7**(5): p. 864-867.
 50. Feng, C., Y. Zhao, and Y.J. Jiang, *Silver nano-dendritic crystal film: a rapid dehydration SERS substrate of totally new concept.* Rsc Advances, 2015. **5**(6): p. 4578-4585.
 51. Gu, H.X., et al., *Facile Fabrication of a Silver Dendrite-Integrated Chip for Surface-Enhanced Raman Scattering.* Acs Applied Materials & Interfaces, 2015. **7**(4): p. 2931-2936.
 52. Zhang, Y.X., et al., *Sulfate-ion-assisted galvanic replacement tuning of silver dendrites to highly branched chains for effective SERS.* Physical Chemistry Chemical Physics, 2014. **16**(35): p. 18918-18925.
 53. Zhang, Y.X., et al., *Magnetic field controlled particle-mediated growth inducing icker-like silver architectures.* Chemical Engineering Journal, 2014. **240**: p. 494-502.

54. Zhao, H., et al., *Green "planting" nanostructured single crystal silver*. Scientific Reports, 2013. **3**.
55. Wang, F., et al., *Tunable growth of nanodendritic silver by galvanic-cell mechanism on formed activated carbon*. Chem. Commun., 2010. **46**(21): p. 3782-3784.
56. Xu, J.C., W.X. Zhang, and Z.H. Yang, *An optical humidity sensor based on Ag nanodendrites*. Applied Surface Science, 2013. **280**: p. 920-925.
57. Avizienis, A.V., et al., *Morphological Transitions from Dendrites to Nanowires in the Electroless Deposition of Silver*. Crystal Growth & Design, 2013. **13**(2): p. 465-469.
58. Cheng, W.M., C.C. Wang, and C.Y. Chen, *The influence of Ni nanoparticles and Ni (II) on the growth of Ag dendrites immobilized on the chelating copolymer membrane*. Materials Chemistry and Physics, 2012. **137**(1): p. 76-84.
59. Liu, R.J., et al., *Polyoxometalate-Assisted Galvanic Replacement Synthesis of Silver Hierarchical Dendritic Structures*. Crystal Growth & Design, 2011. **11**(8): p. 3424-3431.
60. Hsiao, W.H., et al., *Surface-Enhanced Raman Scattering Imaging of a Single Molecule on Urchin-like Silver Nanowires*. Acs Applied Materials & Interfaces, 2011. **3**(9): p. 3280-3284.
61. Yang, Y.J. and G.W. Meng, *Ag dendritic nanostructures for rapid detection of polychlorinated biphenyls based on surface-enhanced Raman scattering effect*. Journal of Applied Physics, 2010. **107**(4).
62. Cheng, W.M., C.C. Wang, and C.Y. Chen, *Preparing chelated copolymer membrane for fabrication of Ag dendrites*. Journal of Colloid and Interface Science, 2010. **348**(1): p. 49-56.
63. Ye, W.C., et al., *Controllable growth of silver nanostructures by a simple replacement reaction and their SERS studies*. Solid State Sciences, 2009. **11**(6): p. 1088-1093.
64. Ren, W., et al., *A Simple Route for the Synthesis of Morphology-Controlled and SERS-Active Ag Dendrites with Near-Infrared Absorption*. Journal of Physical Chemistry C, 2011. **115**(21): p. 10315-10320.
65. Wang, L., et al., *Monodisperse, Micrometer-Scale, Highly Crystalline, Nanotextured Ag Dendrites: Rapid, Large-Scale, Wet-Chemical Synthesis and Their Application as SERS Substrates*. Acs Applied Materials & Interfaces, 2010. **2**(11): p. 2987-2991.
66. Song, J., et al., *Growth of giant silver dendrites on layer-by-layer assembled films*. Polymer, 2015. **63**: p. 237-243.
67. Wang, Y.L., et al., *A Facile, Water-Based Synthesis of Highly Branched Nanostructures of Silver*. Langmuir, 2008. **24**(20): p. 12042-12046.

68. Sun, X.P. and M. Hagner, *Novel preparation of snowflake-like dendritic nanostructures of Ag or Au at room temperature via a wet-chemical route*. Langmuir, 2007. **23**(18): p. 9147-9150.
69. Forati-Nezhad, M., et al., *Affecting the morphology of silver deposition on carbon nanotube surface: From nanoparticles to dendritic (tree-like) nanostructures*. Materials Science & Engineering C-Materials for Biological Applications, 2015. **46**: p. 232-238.
70. Chen, Y.N. and H.L. Wang, *Jellyfish mesoglea as a matrix for the synthesis of extremely high content silver dendrites*. Journal of Colloid and Interface Science, 2015. **454**: p. 14-19.
71. Yang, J.H., et al., *Investigation of the catalysis and SERS properties of flower-like and hierarchical silver microcrystals*. Journal of Nanoparticle Research, 2014. **16**(10).
72. Sivakov, V., et al., *Silver nanostructures formation in porous Si/SiO₂ matrix*. Journal of Crystal Growth, 2014. **400**: p. 21-26.
73. Ng, C.H.B. and W.Y. Fan, *Preparation of Ag Stellar Dendrites: Modeling the Growth of Stellar Snowflakes*. Crystal Growth & Design, 2014. **14**(11): p. 6067-6072.
74. Alam, M.M., et al., *Template free synthesis of dendritic silver nanostructures and their application in surface-enhanced Raman scattering*. Rsc Advances, 2014. **4**(95): p. 52686-52689.
75. Wei, Y.L., et al., *Preparation of dendritic-like Ag crystals using monocrystalline silicon as template*. Materials Research Bulletin, 2011. **46**(6): p. 929-936.
76. Keita, B., et al., *Green Wet Chemical Route for the Synthesis of Silver and Palladium Dendrites*. European Journal of Inorganic Chemistry, 2011(8): p. 1201-1204.
77. Mdluli, P.S. and N. Revaprasadu, *Time dependant evolution of silver nanodendrites*. Materials Letters, 2009. **63**(3-4): p. 447-450.
78. Laurier, K.G.M., et al., *Photocatalytic growth of dendritic silver nanostructures as SERS substrates*. Chemical Communications, 2012. **48**(10): p. 1559-1561.
79. Wang, X., X.H. Liu, and X. Wang, *Self-assembled synthesis of Ag nanodendrites and their applications to SERS*. Journal of Molecular Structure, 2011. **997**(1-3): p. 64-69.
80. Qiao, Y., et al., *Metal-Driven Viscoelastic Wormlike Micelle in Anionic/Zwitterionic Surfactant Systems and Template-Directed Synthesis of Dendritic Silver Nanostructures*. Langmuir, 2011. **27**(5): p. 1718-1723.
81. Yang, C., et al., *A facile chemical approach for preparing a SERS active silver substrate*. Physical Chemistry Chemical Physics, 2010. **12**(43): p. 14459-14461.

82. Tang, S.C., et al., *PVP-assisted sonoelectrochemical growth of silver nanostructures with various shapes*. *Materials Chemistry and Physics*, 2009. **116**(2-3): p. 464-468.
83. Tang, S.C., S. Vongehr, and X.K. Meng, *Two distinct branch-stem interfacial structures of silver dendrites with vertical and slanted branchings*. *Chemical Physics Letters*, 2009. **477**(1-3): p. 179-183.
84. Zhu, J., et al., *Shape-Controlled Synthesis of Silver Nanoparticles by Pulse Sonoelectrochemical Methods*. *Langmuir*, 2000. **16**(16): p. 6396-6399.
85. Zhu, J.J., et al., *Shape-controlled synthesis of silver nanoparticles by pulse sonoelectrochemical methods*. *Langmuir*, 2000. **16**(16): p. 6396-6399.
86. Zhou, Y., et al., *A novel ultraviolet irradiation photoreduction technique for the preparation of single-crystal Ag nanorods and Ag dendrites*. *Advanced Materials*, 1999. **11**(10): p. 850-+.
87. Xia, X., et al., *25th Anniversary Article: Galvanic Replacement: A Simple and Versatile Route to Hollow Nanostructures with Tunable and Well-Controlled Properties*. *Advanced Materials*, 2013. **25**(44): p. 6313-6333.
88. Xu, H.Y., et al., *Surface-enhanced Raman scattering on silver dendrite with different growth directions*. *Journal of Raman Spectroscopy*, 2012. **43**(3): p. 396-404.
89. Zhang, G.X., et al., *Morphology-Controlled Green Synthesis of Single Crystalline Silver Dendrites, Dendritic Flowers, and Rods, and Their Growth Mechanism*. *Crystal Growth & Design*, 2011. **11**(6): p. 2493-2499.
90. Gutes, A., C. Carraro, and R. Maboudian, *Silver Dendrites from Galvanic Displacement on Commercial Aluminum Foil As an Effective SERS Substrate*. *Journal of the American Chemical Society*, 2010. **132**(5): p. 1476-+.
91. Lv, S., et al., *Effect of synthesis route on the morphologies of silver nanostructures by galvanic displacement reaction*. *Solid State Communications*, 2009. **149**(5-6): p. 227-230.
92. Fang, J.X., et al., *How a silver dendritic mesocrystal converts to a single crystal*. *Applied Physics Letters*, 2008. **92**(17).
93. Huang, J., et al., *Ag dendrite-based Au/Ag bimetallic nanostructures with strongly enhanced catalytic activity*. *Langmuir*, 2009. **25**(19): p. 11890-6.
94. Jun Yin, H., et al., *Ag@Au core-shell dendrites: a stable, reusable and sensitive surface enhanced Raman scattering substrate*. *Scientific Reports*, 2015. **5**: p. 14502.
95. Huan, T.N., et al., *Au-Ag bimetallic nanodendrite synthesized via simultaneous co-electrodeposition and its application as a SERS substrate*. *RSC Advances*, 2014. **4**(8): p. 3929-3933.

96. Yi, Z., et al., *Facile preparation of dendritic Ag–Pd bimetallic nanostructures on the surface of Cu foil for application as a SERS-substrate*. Applied Surface Science, 2012. **258**(14): p. 5429-5437.
97. Xia, X., et al., *25th anniversary article: galvanic replacement: a simple and versatile route to hollow nanostructures with tunable and well-controlled properties*. Adv Mater, 2013. **25**(44): p. 6313-33.
98. Wang, T., et al., *The effect of dielectric constants on noble metal/semiconductor SERS enhancement: FDTD simulation and experiment validation of Ag/Ge and Ag/Si substrates*. Sci Rep, 2014. **4**: p. 4052.
99. Yi, Z., et al., *Preparation of dendritic Ag/Au bimetallic nanostructures and their application in surface-enhanced Raman scattering*. Thin Solid Films, 2012. **520**(7): p. 2701-2707.

BIOGRAPHICAL INFORMATION

Sandesh Rajkumar Shelke was born in Maharashtra province, India. He received his B.Tech in Metallurgy and Material Science from College of Engineering, Pune in 2012. He worked for 2 years at JSW Steel Limited as Junior Manager in operation department. After that, he began the study for his master degree in Material Science and Engineering in University of Texas at Arlington in Dr. Yaowu Hao's group. During his master education, he was member of American Society of Materials. His research field was related to the synthesis of silver based bimetallic nanoparticles (gold and palladium) and their applications as SERS substrate. He also worked on different nanomaterials (gold, silver) and its biomedical applications. He is familiar with electro-deposition and electroless plating process for nanostructure. As a master graduate student, he has ability to analyze the different characteristic techniques as Vibrating Sample Magnetometer (VSM) and Raman Spectroscopy.